arXiv:2103.06889v3 [physics.chem-ph] 4 Oct 2021

Multiscale molecular kinetics by coupling Markov state models and reaction-diffusion dynamics

Mauricio J. del Razo[a,b,c,d,1], **Manuel Dibak**[d], **Christof Schütte**[d,e], **and Frank Noé**[d,f,g,1]

[a]Van 't Hoff Institute for Molecular Sciences, University of Amsterdam, The Netherlands; [b]Korteweg-de Vries Institute for Mathematics, University of Amsterdam, The Netherlands; [c]Dutch Institute for Emergent Phenomena, Amsterdam, The Netherlands; [d]Department of Mathematics and Computer Science, Freie Universität Berlin, Germany; [e]Zuse Institute Berlin, Germany; [f]Department of Physics, Freie Universität Berlin, Germany; [g]Department of Chemistry, Rice University, Houston TX, USA

Abstract

A novel approach to simulate simple protein-ligand systems at large time- and length-scales is to couple Markov state models (MSMs) of molecular kinetics with particle-based reaction-diffusion (RD) simulations, MSM/RD. Currently, MSM/RD lacks a mathematical framework to derive coupling schemes; is limited to isotropic ligands in a single conformational state, and is lacking a multi-particle extensions. In this work, we address these needs by developing a general MSM/RD framework by coarse-graining molecular dynamics into hybrid switching diffusion processes. Given enough data to parametrize the model, it is capable of modeling protein-protein interactions over large time- and length-scales, and it can be extended to handle multiple molecules. We derive the MSM/RD framework, and we implement and verify it for two protein-protein benchmark systems and one multiparticle implementation to model the formation of pentameric ring molecules. To enable reproducibility, we have published our code in the MSM/RD software package.

multiscale molecular dynamics | Markov state models | coarse-graining | MSM/RD | hybrid switching diffusions | stochastic reaction-diffusion

I. Introduction

Molecular dynamics (MD) simulations have allowed the study of a broad range of biological systems, from small molecules such as anesthetics or small peptides, to large protein complexes such as the ribosome or even virus capsids (32). One of the main challenges faced by MD simulations is their high computational cost, which can lead to inadequate sampling of conformational states. While there is a large body of research focused on sampling of long-time-scale dynamics of individual macromolecules, there has been less attention on sampling and simulating the interactions of many macromolecules on larger length-scales. This is a more complex problem since it not only involves the long-time dynamics, but it can also involve several orders of magnitude in length-scale. One landmark example is cellular signaling, where relevant processes happen across 6 orders of magnitude in length-scales (0.1 nm–100 µm) and 18 orders of magnitude in time-scales (femtoseconds to hours) (59–61). Two of the most successful approaches to model biomolecular processes at larger time or length-scales are the following:

- Markov state models (MSMs) of molecular kinetics are one of the most well-known techniques to mitigate the MD sampling problem (25, 67, 69, 71–73). They approximate the long-time dynamics of MD systems by Markov chains on discrete partitions of configuration space. This allows to extract the long-time kinetics from short MD trajectories and to calculate molecular observables. State of the art developments have pipelined the MSM approach into deep learning frameworks (46, 66). However, larger and more complex systems require sampling an exponentially growing number of states, constraining its applicability to small domains with one or a few macromolecules.

- Particle-based reaction-diffusion (PBRD) simulations are orders of magnitude more efficient than MD since they model each molecule as one particle undergoing Brownian diffusion. The solvent effects are implicitly modeled through the Brownian noise term (1, 77, 78), and the reactions are regulated by reaction rates. For reactions involving two or more particles, if a pair of reactive particles is close enough to each other, they can react with a certain reaction rate. They are ideal to model multi-particle processes at large length-scales but lack atomic detail. There is a large amount of PBRD literature (3, 5, 6, 13, 14, 16, 41–44, 51), as well as several software packages and simulation schemes (4, 9–12, 15, 28, 40, 53, 76).

By coupling MSMs of molecular kinetics with PBRD, we can combine the best of both worlds and perform multiscale molecular simulations across large time and length-scales; we call this coupling MSM/RD. However, this coupling is not trivial. The existing implementation of MSM/RD in (30) suffered from several limitations: there was no underlying mathematical theory to justify and derive the coupling scheme; it was limited to simple ligand-protein systems; the protein was assumed fixed in the frame of reference; the ligand orientation and possible conformation switching was not taken into account; and multiparticle extensions were not implemented. However, the aim of MSM/RD remains the same, to produce efficient multiscale simulations that reproduce the essential statistical behavior of a practically unaffordable large-scale MD simulation by employing only statistics obtained from simulations of the constituent molecules in small solvent boxes.

In this work, we develop a general framework for MSM/RD that overcomes the previous shortcomings. It is derived by coarse-graining molecular kinetics into hybrid switching diffusion processes (22, 23), also known as diffusion processes with Markovian switching. These correspond to a class of stochastic hybrid systems, called "hybrid" due to the coexistence of continuous dynamics and discrete events in the same process. The molecules diffusion corresponds to the continuous part, while

M.J.R., C.S. and F.N. designed research; M.J.R. and M.D. performed research; M.J.R. and F.N. wrote the paper.

The authors declare no conflict of interest.

[1] E-mails: maojrs@gmail.com and frank.noe@fu-berlin.de

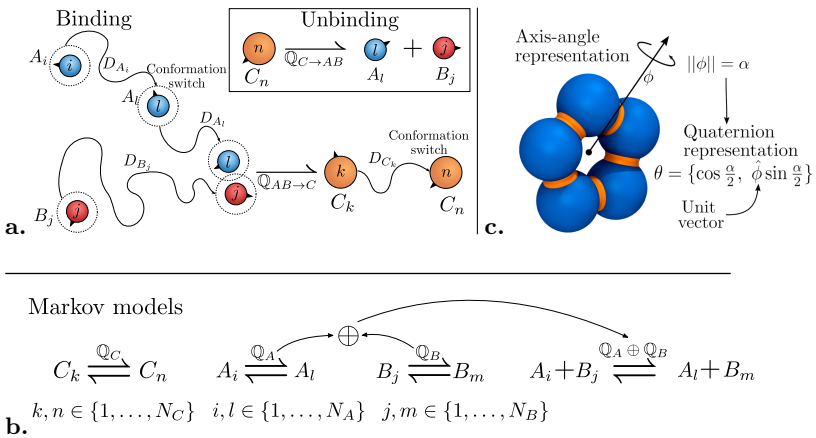


Fig. 1. Diagrams to illustrate MSM/RD theory and general rotations. **a.** Diagram of the binding and unbinding of two reactive molecules, $A + B \rightleftharpoons C$, when modeling their kinetics as hybrid switching diffusions. Molecules are represented by particles with position and orientation (black pointer). The three molecules have a conformation-dependent diffusion, and the conformations are denoted by a subindex. If molecules A and B are close enough to each other, they transition to a bound compound C with a configuration-dependent rate given by $\mathbb{Q}_{AB\to C}$. The compound C can also unbind into molecules A and B with a configuration-dependent rate given by $\mathbb{Q}_{C\to AB}$. **b.** Diagram showing the individual Markov models for C,A and B, and the Markov model for the joint system of molecules A and B when not interacting. **c.** Orientation of a pentameric ring molecule using the axis-angle representation with the molecule's center as reference. The direction of the ϕ vector,$\hat{\phi}$, represents the axis of rotation, and its magnitude $||\phi|| = \alpha$ represents the radians to be rotated. We can translate this to its quaternion representation.

their conformation switching corresponds to the discrete part. By discretizing the framework, we derive MSM/RD schemes; we implement and validate them for two protein-protein benchmark systems and one multiparticle implementation to model the formation of pentameric ring molecules. Implementations in more realistic systems are left for future work. However, given enough data to parametrize the model, the framework is ideal for applications on protein-ligand and protein-protein dynamics, as well as self-assembly of structures composed of several copies of the same or a small set of molecules, such as virus capsids.

Previous relevant works (17–19) introduced spatially dependent reaction rates, a fundamental concept in our framework and (7, 8, 33, 34, 45) have modeled fluctuations on the reactivity of the species using Markovian gates, a special case of our framework. A related multiscale method (28, 53) couples MD with Green's function reaction dynamics, including anisotropic interactions. Although still constrained by MD computations, this method could potentially be combined with our approach to accelerate both MD and PBRD simulations. The work (56) provides an excellent review on several multiscale methods for protein-ligand binding, including (57, 58), where multiscale simulations are used to estimate kinetic rates. The ideas presented in this work could help enhance these methods. Moreover, references (35–39) have focused on implementing several stochastic hybrid models in different fields in biology, which emphasizes the relevance of stochastic hybrid models in biological settings. Note hybrid switching diffusions are a general coarse-grained model of MD, and they can thus be applied to many other applications beyond MSM/RD, such as the diffusion and conformation switching of molecules under a concentration or temperature gradient.

II. Molecular kinetics as hybrid switching diffusions

A. One molecule. Consider a molecule A. If we fix the position and orientation of the molecule, the position of its atoms only change due to conformational changes. We can then coarse-grain the all-atom dynamics in configuration space into an MSM (24, 25, 73). Let us assume our molecule A can be described by switching between two MSM states $A_1 \rightleftharpoons A_2$.

If molecule A is now diffusing instead of being fixed in space, we would expect different diffusion coefficients in different conformations. The diffusion and the conformation switching can be modeled together,

$$\frac{\partial}{\partial t}\begin{bmatrix} p_1 \\ p_2 \end{bmatrix} = \begin{bmatrix} D_1\nabla^2 p_1 \\ D_2\nabla^2 p_2 \end{bmatrix} + \begin{pmatrix} -r_{12} & r_{21} \\ r_{12} & -r_{21} \end{pmatrix}\begin{bmatrix} p_1 \\ p_2 \end{bmatrix},$$

where $p(x,t)$ is the vector of probability densities $(p_1, p_2)^T$ of being in conformation A_1 or A_2 at position x, r_{ij} are the transition rates from conformation A_i to A_j that form the corresponding transition rate matrix. Note the first term of the right hand side corresponds to the Fokker-Planck equations of the diffusion processes, while the second term corresponds to a continuous-time MSM, or Master-equation model (24). We would like to incorporate rotational diffusion and generalize it to N different conformations. The resulting generalization yields

$$\frac{\partial p(x,t)}{\partial t} = \underbrace{\mathcal{D}p(x,t)}_{\text{Diffusion}} + \underbrace{\mathbb{Q}p(x,t)}_{\text{MSM}}, \qquad [1]$$

where $p(x,t) = (p_1, \ldots, p_N)^T$ is the vector of probability densities of being in the corresponding conformations at x and time t, with $x = (r, \theta)$ denoting the position and orientation coordinates of the molecule. The operator $\mathcal{D}$ describes the translational and rotational diffusion of the molecule in each of its conformations. The matrix $\mathbb{Q}$ is a $N \times N$ transition rate matrix describing the conformation switching; its diagonal entries are all negative and its non-diagonal ones positive; its columns sum to zero. In this way, the equation models simultaneously the molecule's diffusion and the switching of conformation. Equation 1 is an example of a hybrid switching diffusion process, and one could also write a stochastic differential equation for the individual stochastic trajectories. A detailed derivation of this theory is presented in the SI Appendix A. The diffusion operator and the transition rate matrix can be a function of x, $\mathcal{D}(x)$ and $\mathbb{Q}(x)$, which provides a robust framework for several interesting applications. In this work, we are interested in the interaction between two molecules, so we generalize this result for two interacting molecules.

B. Two interacting molecules. Consider two molecules A and B. If they are far enough from each other, they will not interact. Each molecule has a state vector assigned, p_A and p_B, with sizes N_A and N_B corresponding to their respective number of conformations. The conformations are denoted by A_i and B_j with $i = 1, \ldots, N_A$ and $j = 1, \ldots, N_B$. The diffusion operators $\mathcal{D}_A$ and $\mathcal{D}_B$ encode the rotational and

translational diffusion, which in the simplest case will correspond to Laplacian operators with diffusion coefficients for the different conformations, D_{A_i} and D_{B_j}. The rate matrices $\mathbb{Q}_A$ and $\mathbb{Q}_B$ encode the rates at which they switch conformation. Each molecule will satisfy its own version of Eq. 1

$$\frac{\partial p_A}{\partial t} = \mathcal{D}_A p_A + \mathbb{Q}_A p_A, \qquad \frac{\partial p_B}{\partial t} = \mathcal{D}_B p_B + \mathbb{Q}_B p_B, \quad [2]$$

see Fig. 1a for a graphical reference. The state of the system p_{AB} is given by all the possible combinations of states of A and states of B. This corresponds to the tensor product of all the states of A with all the states of B, i.e. $p_{AB} = p_A \otimes p_B$ (62). For instance, if A and B have two states each, A_1, A_2 and B_1, B_2 respectively, the full system given by the tensor product has four possible states: A_1B_1, A_1B_2, A_2B_1 and A_2B_2. Taking the time derivative of $p_A \otimes p_B$ and using Eqs. 2, we obtain

$$\frac{\partial p_{AB}(x)}{\partial t} = \mathcal{D} p_{AB}(x) + (\mathbb{Q}_A \oplus \mathbb{Q}_B)\, p_{AB}(x), \quad [3]$$

where the diffusion operator is applied independently before taking the tensor product $\mathcal{D}p_{AB} = \mathcal{D}_A p_A \otimes p_B + p_A \otimes \mathcal{D}_B p_B$ and $\mathbb{Q}_A \oplus \mathbb{Q}_B = (\mathbb{Q}_A \otimes \mathbb{I}_{N_B}) + (\mathbb{I}_{N_A} \otimes \mathbb{Q}_B)$ is the Kronecker sum with $\mathbb{I}_K$ the identity matrix of order K. The appearance of the Kronecker sum results evident when computing the solution of the full system as the tensor product of the individual solutions of Eqs. 2, $p_{AB}(x,t) = e^{t\mathcal{D}_A} \otimes e^{t\mathcal{D}_B} \otimes e^{t(\mathbb{Q}_A \oplus \mathbb{Q}_B)} p_{AB}(x,0)$ (62). This means that the rate matrix of the full system is given by the transition rate matrix $\mathbb{Q}_A \oplus \mathbb{Q}_B$ (Fig. 1b). Note that if we were using a discrete-time MSM, the transition probability matrix of the full system will simply be the tensor product of the independent transition probability matrices.

Let's assume now molecules A and B are close to each other and are interacting, such that they can be considered as a complex C that diffuses as a single entity. The state vector is p_C with dimension N_C, corresponding to the bound conformations, C_k with $k = 1, \ldots, N_C$. We can thus write it in the form of Eq. 2

$$\frac{\partial p_C}{\partial t} = \mathcal{D}_C p_C + \mathbb{Q}_c p_C. \quad [4]$$

We would like to switch smoothly between the non-interacting regime (Eq. 3) and the bound regime (Eq. 4), so we introduce a transition regime, where the molecules are still dissociated but interacting, and the transition rates strongly depend on the relative position and orientation between the molecules. The dynamics of the system in the three regimes can be written in terms of the probability of being in any of the dissociated states (AB) (Eqs. 3) and any of the bound states (C) (4), namely $p(x,t) = (p_{AB}, p_C)^T$, and a transition rate matrix $\mathbb{Q}(x)$ that depends on the phase space coordinates x, more specifically on the relative position and orientation between the molecules. We can write the dynamics of $p(x,t)$ as a hybrid switching diffusion process

$$\frac{\partial p(x)}{\partial t} = \mathcal{D} p(x) + \mathbb{Q}(x) p(x), \quad \mathbb{Q}(x) = \left(\begin{array}{c|c} \mathbb{Q}_{AB} & \mathbb{Q}_{C\to AB} \\ \hline \mathbb{Q}_{AB\to C} & \mathbb{Q}_C \end{array} \right). \quad [5]$$

The matrix $\mathbb{Q}_{AB\to C}$ contains the transition rates from dissociated states (AB) to bound states (C), and vice versa for the matrix $\mathbb{Q}_{C\to AB}$. If the initial relative distance between the molecules is large enough, the molecules are in the non-interacting regime; $\mathbb{Q}_{AB\to C}$ is zero; the system can only reach the states accessible by $\mathbb{Q}_A \oplus \mathbb{Q}_B$ –so $\mathbb{Q}_{AB} = \mathbb{Q}_A \oplus \mathbb{Q}_B$– and the dynamics given by Eq. 3 are recovered. However, diffusion can bring the molecules together into the transition regime, making $\mathbb{Q}_{AB\to C}$ nonzero and allowing the system to transition to the bound regime. The system can then transition to other bound states through $\mathbb{Q}_C$, and it can transition out of the bound regime into the transition regime (dissociated) through $\mathbb{Q}_{C\to AB}$. Note columns of $\mathbb{Q}(x)$ should sum to zero for any given x, and $\mathbb{Q}_C$ on Eq. 5 is a renormalized version of $\mathbb{Q}_c$ in Eq. 4.

Equation 5 constitutes the general MSM/RD framework, and its dynamics are represented in Figs. 1a and 1b. The SI Appendix A.3 shows a more detailed derivation of this theory. Discretizations of this model are used to generate MSM/RD schemes. In the methods section, we derive the MSM/RD schemes used throughout this work by doing a piecewise constant discretization of $\mathbb{Q}(x)$. Their parametrization and explicit algorithms are given in the SI appendices B and C.

C. Quaternions . The MSM/RD framework requires a representation for the orientation or rotation θ of a rigid body, such as: Euler angles, rotation matrices or unit quaternions among others. Some of these have severe disadvantages, such as the gimbal lock in Euler angles, while unit quaternions have proved to be the most simple, robust and numerically efficient (27–29, 47). A quaternion $\theta = \{s, p\}$, consists of a real part s and a three-dimensional vector part p. If normalized to one, $s^2 + p \cdot p = 1$, it can be used to represent a three-dimensional rotation. Let us consider first a more physically intuitive representation of rotations, the axis-angle representation, where an arbitrary rotation is represented by a three dimensional vector ϕ (Fig. 1c). Its direction $\hat{\phi} = \phi / \|\phi\|$ corresponds to the axis of rotation following the right hand rule, and the length of the vector $\|\phi\|$ corresponds to the magnitude of rotation (Fig. 1c). The corresponding quaternion associated to this rotation is

$$\theta = \{\cos(\|\phi\|/2),\ \sin(\|\phi\|/2)\,\hat{\phi}\}. \quad [6]$$

Similar to complex numbers, quaternions are further endowed with an algebraic structure such that the resulting rotation of consecutive rotations, θ_1 and θ_2, is obtained by an algebraic multiplication, $\theta = \theta_2 \theta_1$,

$$\theta = \{s_2 s_1 - p_2 p_1,\ s_2 p_1 + s_2 p_1 + p_2 \times p_1\},$$

where the cross product makes the multiplication non-commutative, as expected for rotations. The unit quaternion $\theta^{-1} = \{s, -p\}$ is the inverse quaternion of θ representing the inverse rotation, such that $\theta\theta^{-1} = I$ is the identity rotation. Note the quaternion $-\theta$ corresponds to the same rotation as θ; therefore it is enough to use half of the surface of the four-dimensional unit sphere to describe all possible rotations in three-dimensional space. If a one to one relation is desired, the simplest choice is to restrict to $s \geq 0$. More detailed accounts of quaternions can be found in the literature (27–29).

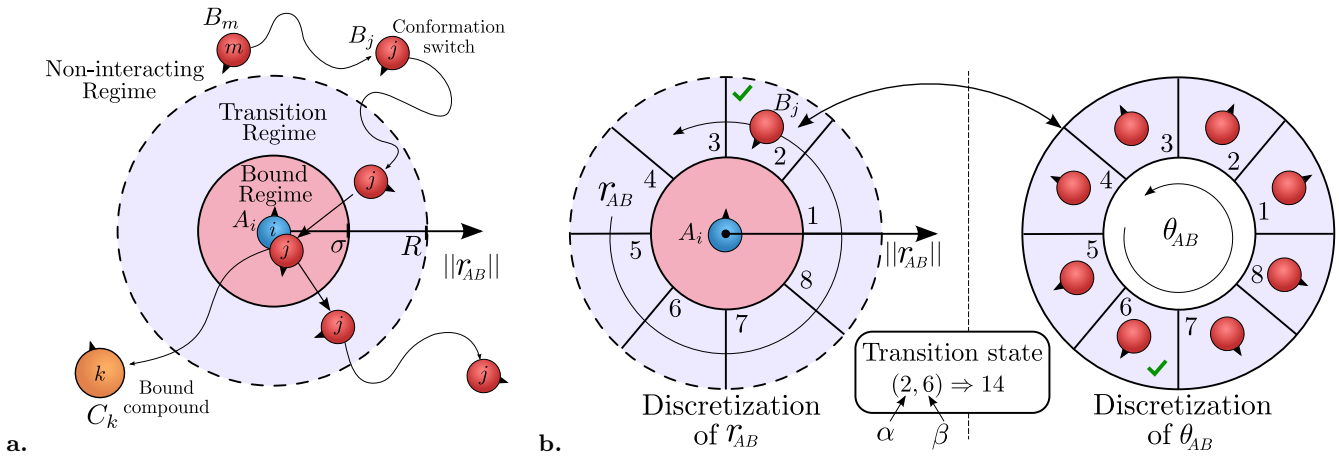


Fig. 2. Discretization diagrams for the MSM/RD scheme **a.** Diagram of the three different regimes in the MSM/RD scheme defined by $\sigma < \|r_{AB}\| < R$. The bound regime is shaded in red; the transition regime is shaded in blue and the non-interacting regime is in white. To define these regions, we fix the frame of reference to molecule A. In the non-interacting regime, they both diffuse and change conformation freely. In the transition regime, they can transition to a bound compound state. From the bound state, they can unbind and switch to a specific configuration in the transition regime. From the transition regime, they can diffuse away into the non-interacting regime. Note the orientation is specified by a small black pointer attached to each particle. **b.** Definition of transition states (or unbound transition states) within the transition regime. To define the transition states, we perform two discretizations: one for the relative position r_{AB} and one for the relative orientation θ_{AB}. In this illustration, the relative position is simply a two dimensional vector, so we simply partition the blue shaded ring ($\sigma < \|r_{AB}\| < R$) from 0 to 2π into 8 parts. For each discrete value of the relative position, the molecules can still have an arbitrary relative orientation, so, we also need to discretize the relative orientation. The relative orientation is represented with one degree of freedom, so we discretize it by partitioning the circle into 8 parts. If α is the discretization state of r_{AB} and β the one of θ_{AB}, the transition state number is given by $(\alpha - 1)8 + \beta$. This discretization yields a total of $8 \times 8 = 64$ transition states. In each transition state, the rates are approximated by a constant value, yielding a piecewise constant approximation of the rates in $\mathbb{Q}$. In our MSM/RD implementation, an analogous discretization is done in three dimensions (six degrees of freedom).

III. Methods

A. A general MSM/RD scheme . The general MSM/RD framework for two interacting molecules is condensed in Eq. 5. In most cases, we will not know the rate functions constituting Eq. 5. However, we can discretize the equation and obtain a specific MSM/RD coupling scheme, which can be parametrized with MD trajectories. Equation 5 thus provides a robust theoretical foundation from which different MSM/RD schemes can be derived by applying different discretizations; it serves as a guideline to derive different and better suited schemes for the situation at hand.

The MSM/RD schemes used throughout this work originate from piecewise constant discretizations of the transition rate matrix $\mathbb{Q}(x)$ from Eq. 5. We first divide the phase space in the three main regions/regimes: non-interacting, transition and bound regimes (Fig. 2a). The definition of these regimes will be system dependent and based on the relative position between the two molecules. As a rule of thumb, the interaction between molecules must be weak in the transition regime and effectively zero in the non-interacting regime. MSM/RD requires parametrizing two MSMs, one for the non-interacting regime, $\mathbb{Q}_A \oplus \mathbb{Q}_B$, and one for the transition and bound regime together. In the sections below, we will cover how the MSM/RD dynamics are constructed in each of these regions. In the SI Appendices C and B, we further show the corresponding MSM/RD algorithm and how to discretize the MD trajectories to parametrize the MSM/RD scheme.

Non-interacting regime. We consider two molecules A and B as rigid bodies with relative position $r_{AB} = r_B - r_A$, and relative orientation $\theta_{AB} = \theta_B \theta_A^{-1}$, where θ_A and θ_B are quaternions representing orientations. Following Eq. 2, if the two molecules are far enough apart, $\|r_{AB}\| \geq R$, they diffuse and change conformation independently. Thus the rates of the transition matrix $\mathbb{Q}(x)$ do not depend on r_{AB} or θ_{AB}, and the dynamics of the individual molecules are discretized into individual MSMs using standard methods (73), yielding $\mathbb{Q}_{AB} = \mathbb{Q}_A \oplus \mathbb{Q}_B$. For the sake of simplicity and without loss of generality, we assume the particles are modeled with overdamped Langevin dynamics. The corresponding SDE based on S9 is

$$\frac{dX_k(\eta_k, t)}{dt} = \sqrt{2k_B T} M_k^{\frac{1}{2}}(\eta_k)\xi(t), \qquad [7]$$

where k denotes the molecule A or B; $dX_k = [dr_k, d\Phi_k]$, with dr_k the change in position of molecule k and $d\Phi_k$ its change of orientation in the axis-angle representation; M_k the mobility matrix of molecule k, which depends on its conformation η_k; and $\xi(t)$ corresponds to six-dimensional Gaussian white noise. The conformation η_k of each molecule changes following a discrete- or continuous-time MSM with the constant rates from the transition matrix $\mathbb{Q}_A \oplus \mathbb{Q}_B$. Thus, η_k can be propagated by simply sampling transition probabilities in the discrete case or by using a Gillespie-type algorithm(2, 20) in the continuous case. This description corresponds to the trajectory representation of the stochastic process described by Eq. 2. If the translational and rotational motion are weakly coupled and both isotropic, we can approximate Eq. 7 by

$$\frac{dr_k(\eta_k, t)}{dt} = \sqrt{2D_k(\eta_k)}\xi(t), \qquad [8]$$
$$\frac{d\Phi_k(\eta_k, t)}{dt} = \sqrt{2D_k^{\mathrm{rot}}(\eta_k)}\xi_{\mathrm{rot}}(t),$$

where D_k and $D_k^{\mathrm{rot}}$are the translation and rotational diffusion coefficients of molecule k, and in these equations, $\xi(t)$ and $\xi_{\mathrm{rot}}(t)$ each correspond to three-dimensional Gaussian white noise. Note in this region the C states are not accessible, so only $\mathbb{Q}_{AB}$ is relevant. The numerical discretization of this equation has the same form as Eq. 11 but with zero force and torque terms. The diffusion coefficients (or matrices in the general case) should also be estimated from MD trajectories.

There are several works focused on this topic (47–49); we also added a small section about it in the SI Appendix D.

Transition regime. The transition regime is defined by the region between the non-interacting and the bound regime, $\sigma < \|r_{AB}\| < R$. In this regime, the transition rates depend continuously on the relative position and orientation of the molecules. As we plan to infer these rates from MD simulations, it is convenient to discretize $\mathbb{Q}(x)$ into a relatively small number of transition regions/states where the rates are approximated by constant values, yielding a piecewise constant approximation of $\mathbb{Q}(x)$ that is easier to infer from MD data.

Figure 2 shows an illustration of the different regions/states and the discretization of the transition regime for a simplified lower dimensional case. For each transition state, given by the combination of a discrete value of the relative position and of the relative orientation, we approximate the rates in $\mathbb{Q}(x)$ by a constant value, yielding a piecewise constant approximation of $\mathbb{Q}_{AB}$ and $\mathbb{Q}_{AB\to C}$ in the transition regime. In this regime the particles are always dissociated, so $\mathbb{Q}_{C\to AB}$ and $\mathbb{Q}_C$ are not relevant.

In general, the relative position and the relative orientation account for a total of six degrees of freedom, so the discretization of the transition regime is much more complex than in Fig. 2, but it still follows the same principle. The first step is to provide an equal area partition of the surface of the sphere following (31), yielding a discretization of the relative position in the transition region. Then, we need to discretize the relative orientation, which is given in terms of a unit quaternion. As unit quaternions can be projected into the top half three dimensional unit sphere, we use the same equal area partition sphere with a few additional cuts along the radial direction, yielding an effective discretization of all the possible relative orientations. It is important to keep the number of divisions in these partitions as small as possible to avoid an exploding number of transition states.

Note conformation switching within the transition regime is naturally incorporated in the framework. The transition matrix $\mathbb{Q}(x)$ acts on $p(x,t) = (p_{AB}, p_C)^T$, where p_{AB} includes one entry for every possible conformation combination between the two molecules. Thus, the discretization of $\mathbb{Q}(x)$ includes the rates corresponding to conformation changes within the transition regime. Alternatively, by collapsing all conformations into one state in the parametrization, one can obtain averaged rates over all conformations for all the transitions within the transition regime.

In the transition regime, the diffusion of the particles —approximated by Eq. 7— and the propagation of the MSM —following $\mathbb{Q}_{AB}$ and $\mathbb{Q}_{AB\to C}$— are run in parallel. If $\|r_{AB}\|$ becomes larger than R due to diffusion, the MSM is ignored and the dynamics switch to the non-interacting regime. If a binding event occurs, the diffusion of the binding particle is ignored and the dynamics switch to the bound regime.

Bound regime. If molecules A and B are close enough to each other, $\|r_{AB}\| \leq \sigma$, they are strongly interacting and can be considered as a bound compound C with several metastable configurations. In this case, their diffusion and conformation switching are no longer independent, and the transition rates do not depend on r_{AB} and θ_{AB}, so they are assumed constant. The transitions in the bound regime can be between metastable states (following $\mathbb{Q}_C$) or towards an unbound state in the transition regime (following $\mathbb{Q}_{C\to AB}$). Analogously to the previous example, we assume without loss of generality that the dynamics of the compound follow overdamped Langevin dynamics

$$\frac{dX_C(\eta_C, t)}{dt} = \sqrt{2k_BT}M_C^{\frac{1}{2}}(\eta_C)\xi(t), \qquad [9]$$

with $dX_C = [dr_C, d\Phi_C]$. The conformation η_C is propagated using the rates from $\mathbb{Q}_C$ and $\mathbb{Q}_{C\to AB}$. The dynamics are propagated in the same way as Eq. 7. If the translational and rotational motion are weakly coupled and isotropic, we can obtain analogous results to that of Eq. 8 with $k = C$ and with analogous numerical discretization and diffusion coefficient estimation. If a transition towards a dissociated state in the transition regime happens, the dynamics switch to the transition regime. In the bound regime, particles are always bound, so $\mathbb{Q}_{AB\to C}$ and $\mathbb{Q}_{AB}$ are not relevant. Note when parametrizing $\mathbb{Q}(x)$ from MD data, we obtain one MSM at once for both the transition and bound regime (SI appendix B), which describes all states in which A and B are interacting, including strongly and weakly bound states, intermediates between unbound and bound state and even dissociated states in which A and B are sufficiently close to induce a force upon each other. Such MSMs have, for example, been computed for protein-ligand and protein-protein association in the past few years (68, 70, 74, 75).

B. Benchmark MD model: patchy particles . To validate MSM/RD schemes, we require an inexpensive model of molecules capable of representing complex behavior observed in realistic MD systems such as: translational and rotational diffusion, position and orientation dependent pair interactions, orientation dependent binding, multiple binding sites and conformation switching. We can construct such a model based on patchy particles (26, 52, 54). We model molecules as diffusive spherical particles with an isotropic repulsive potential $U_{\text{isotropic}}$ to avoid overlapping; an attractive isotropic part can also be incorporated. Patches are then placed on the surface of the particles, and each patch produces a short-range attractive potential with patches from other particles, generating translational and rotational motion (28). The potential energy between patch i of particle A and patch j of particle B can be decomposed into two parts. The first part U_r^{ij} depends only on the relative distance between the patches, r_{ij}, and the types of the patches. It corresponds to an attractive force that pulls patches together . The second part U_θ^{ij} depends on the relative orientation, θ_{AB}, of the particles, and it is activated if two patches are close enough to each other. This will favor specific relative orientations for the different bindings between patches. In all the models used for this work, the overall interaction potential between two particles, A and B, can be written in the following form:

$$U_{AB} = U_{\text{isotropic}}(r_{AB}) + \sum_{i,j=1}^{N_A,N_B} \left(U_r^{ij}(r_{ij}) + U_\theta^{ij}(r_{ij}, \theta_{AB})\right),$$

where i runs over the patches of particle A and j runs over the patches of particle B. N_A and N_B are the total number of patches of A and B respectively. In general, particle A and B can both have conformational changes; each combination of conformations is allowed to have a completely different potential energy. In this work, conformation changes will

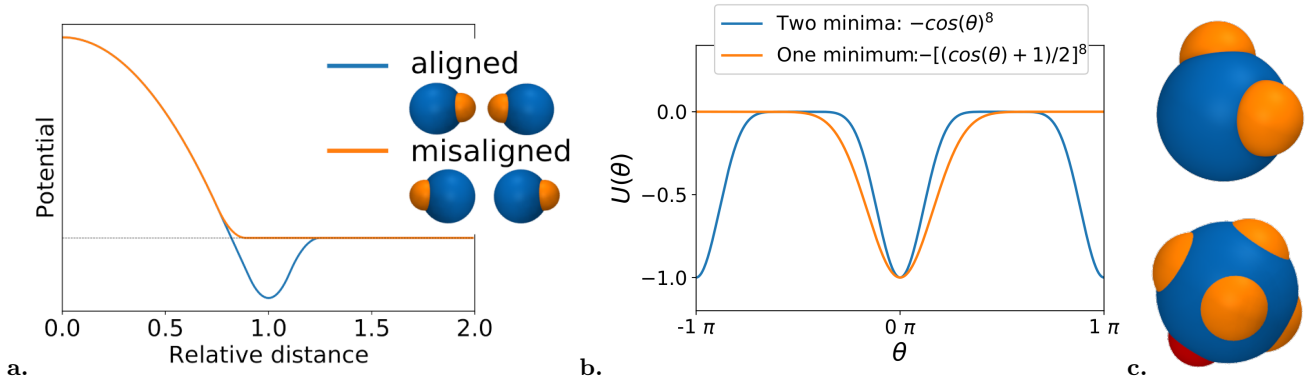


Fig. 3. Illustration of the patchy particle potential. **a.** This plot shows the patchy particle potential between two particles with a diameter of one, each with one patch. The potential is plotted as a function of the relative distance between the two particles for orientations corresponding to aligned or misaligned patches. If aligned, we observe a stable minimum in the potential corresponding to particles binding. If misaligned, there is no stable minimum, and the isotropic repulsion prevents overlapping. See (28) for the specific form of the potential. **b.** Two examples of angular potentials used in this work, corresponding to one and two metastable orientations. As the bindings between patches already fix two orientational degrees of freedom, we only require a one dimensional angular potential to completely fix the orientation. **c.** Examples of patchy particles with two and six patches. The patches can also be of different types corresponding to different interaction potentials, and they can be turned on an off depending on the current conformation.

correspond to turning on and off specific patches. Figure 3 shows the potential between a pair of patchy particles with one patch, as well as examples of orientation dependent potentials.

The position of the particles is simply given by the coordinates of the center of the sphere $r(t)$, and their orientation $\theta(t)$ is given in terms of quaternions. In order to model the translational and orientational diffusion of one particle, we use overdamped Langevin dynamics. We assume the translational and rotational diffusion are independent and both isotropic, so we obtain

$$\begin{aligned}\frac{dr(t,\eta)}{dt} &= \frac{1}{\gamma}F(r,\eta) + \sqrt{2D(\eta)}\xi(t),\\ \frac{d\Phi(\eta,t)}{dt} &= \frac{1}{\gamma_{\text{rot}}}\mathrm{T}(\theta,\eta) + \sqrt{2D^{\text{rot}}(\eta)}\xi_{\text{rot}}(t)\end{aligned} \qquad [10]$$

where Φ is the orientation in the axis-angle representation, γ and γ_{rot} are the translational and rotational damping coefficients; F and T the force and torque due to pair-interactions and external fields; η is the conformation of the particle; and $\xi(t)$ and $\xi_{\text{rot}}(t)$ each correspond to three-dimensional Gaussian white noise. The force can be rewritten in terms of the potential as $F = -\nabla U$; the torque is convenient to leave explicitly since it is not trivial to write a potential in terms of axis-angle variables or quaternions. These two equations can be discretized using the Euler-Maruyama scheme (21) using a time-step δt.

$$\begin{aligned}r(t+\delta t,\eta) &= r(t,\eta) - \frac{\delta t}{\gamma}\nabla U(r,\eta) + \sqrt{2D(\eta)\delta t}\mathcal{N}(0,1),\\ d\Phi(t,\eta) &= \frac{\delta t}{\gamma_{\text{rot}}}\mathrm{T}(\theta,\eta) + \sqrt{2D^{\text{rot}}(\eta)\delta t}\mathcal{N}(0,1).\end{aligned} \qquad [11]$$

The rotation represented by the change in axis-angle $d\Phi(t)$ can be rewritten as a quaternion $d\theta(t)$ using Eq. 6. The new orientation is simply given by the quaternion product $\theta(t+\delta t) = d\theta(t)\theta(t)$. In each case, $\mathcal{N}(0,1)$ represents an independent three-dimensional vector with each entry a normal random variable with mean zero and variance 1. As the diffusion coefficients depend on the conformation, it is convenient to assume the switching of conformation η is modeled with an MSM using a fixed lag-time τ that is a multiple of $\tau = n\delta t$, n a positive integer. This is not strictly required, but it simplifies the implementation since the conformation change occurs always at the end of a time step. The forces and torques are calculated directly from potential energies like the ones shown in Fig. 3.

This model satisfies all the requirements we established at the beginning of this section. It can be generalized to non-isotropic and coupled rotational and translational dynamics (27, 54), and molecules can even be modeled by multiple overlapping beads with reaction patches (54).

IV. Results

To test and verify MSM/RD, we construct an MD benchmark model of molecules that is simple enough such that we can produce a large amount of data, but complex enough so it models complex behavior observed in realistic MD systems. This model is based on patchy particles (26, 52, 54); we model molecules as spherical particles with isotropic diffusion and an isotropic repulsive potential to avoid overlapping. Patches are then placed on the surface of the particles, and each patch produces a short-range configuration-dependent attractive potential with patches from other particles, generating translational and rotational motion, see the methods section for details. This model is the basis for all the benchmark models in this section.

In the following examples, it is not necessary to parametrize the diffusion operator since it is the same for both the benchmark and the MSM/RD simulation. This serves to isolate the dynamics of $\mathbb{Q}(x)$ and validate the coupling mechanism. For general protein-protein systems, one needs to extract the diffusion coefficients/matrices from the MD data using well documented methods (47, 48) (SI Appendix D).

A. MSM/RD for protein-protein systems . The benchmark model consists of two molecules, A and B (Fig. 4a), represented by different patchy particles. Particle A has only one conformation and six binding patches: five of them have the same attraction potential (yellow), and the other one has a stronger attraction potential (red). Particle B has two conformations. In one conformation (B), it has one binding patch (red), and in the other one (B^*), the patch is turned off, and it

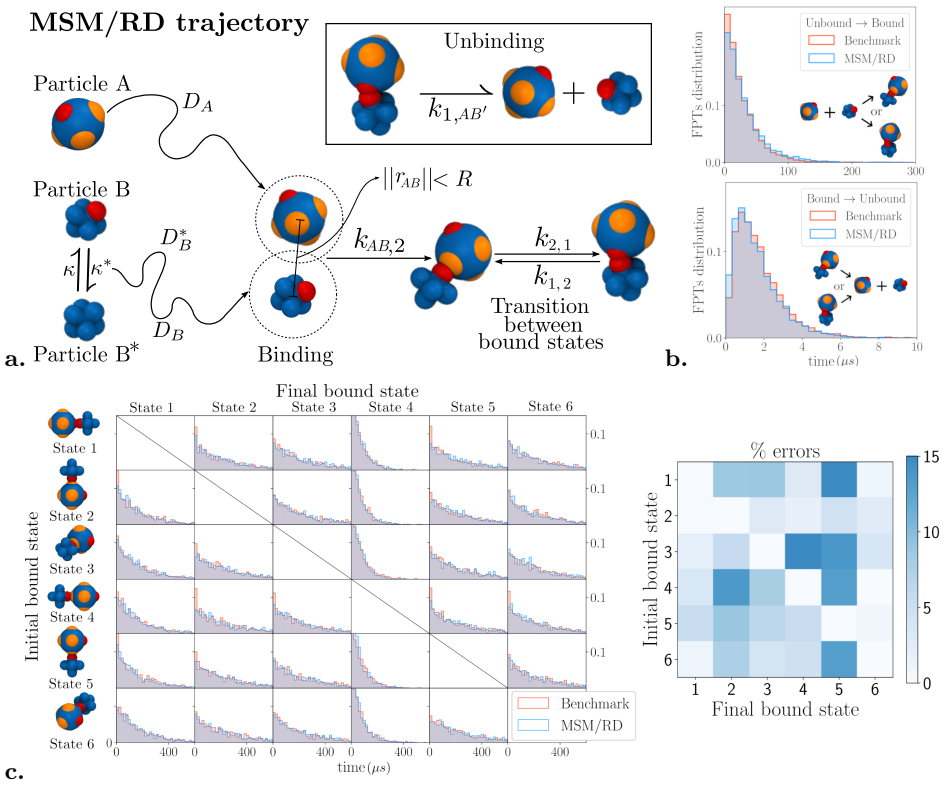


Fig. 4. Illustrations and results of the MSM/RD scheme for the protein-protein system. **a.** MSM/RD sample trajectory. Particle A diffuses with coefficient D_A, and particle B with coefficient D_B or D_B^* depending on its conformation. If the relative distance satisfies $\|r_{AB}\| < R$, we switch from the non-interacting to the transition regime. Here, the particles can transition to one of the six bound states with rate $k_{AB,n}$ that depends on their relative configuration $x_{AB} = (r_{AB}, \theta_{AB})$ and the final bound state $n = 1, \dots 6$. From a bound state n, the compound can transition to another bound state m with rate $\kappa_{n,m}$, or it can unbind to another relative configuration x'_{AB} with rate $k_{n,AB'}$. MSM/RD provides a piecewise constant approximation of all the configuration-dependent rates. **b.** Comparisons of first passage time (FPT) distributions between the benchmark and MSM/RD from an unbound state to any bound state and vice versa. Each distribution was calculated with 5000 simulations. **c.** Comparison of FPT distributions for all transitions between the six possible bound states, each calculated over 1000 simulations. The blue grid shows the relative error of the corresponding rates, $\kappa_{n,m}$, calculated as the inverse MFPT. The average percentage error is of 5%,while the maximum is of 16%.

cannot bind. Each binding allows only one meta-stable relative orientation, yielding a total of six possible bound states. The diffusion of B depends on its conformation, and it is visualized as a three-dimensional asterisk to distinguish its orientation. We illustrate an MSM/RD trajectory of the system on Fig. 4a.

To parametrize the MSM/RD scheme, we simulate the benchmark MD model with specific settings to mimic a common MD simulation. We assume both molecules have a diameter of $5\,nm$, which is a typical size for a real protein. We simulate using periodic boundary conditions and a cube with edge-length of 25nm as unit cell. Each simulation runs for 6×10^6 time steps of $1{\times}10^{-5}\mu s$ each, yielding a total simulation time of $60\mu s$. We run 600 of these simulations independently, and we use them to parametrize the MSM/RD scheme following the steps illustrated in SI Appendix B.

In Fig. 4, we compare the MSM/RD results against the MD benchmark. We calculate the first passage times (FPTs) of a given transition by running the benchmark and the MSM/RD simulations in equal conditions, and we run the same number of FPT samples for each model. Figure 4b compares the FPTs distribution from the unbound state to any bound states and vice versa. The left panel of Fig. 4c compares the FPT distributions for all the possible transitions between bound states. Note these transitions include pathways that start at a bound state, unbind completely and end in another bound state, so it is ideal to evaluate if the MSM/RD produces an accurate coupling. The right panel of Fig. 4c shows the MSM/RD scheme percent error for the transition rates between bound states. Overall, MSM/RD can reproduce the dynamics of the MD benchmark with good accuracy.

B. MSM/RD for dimer of two-patch particle . The benchmark model consists of two identical molecules, each with two equally strong binding patches. The molecules can bind together through any of their two binding sites. Unlike the previous example, we allow for two meta-stable relative orientations per patch binding, allowing for a conformation change in the bound configuration.

As the molecules have two patches each, they can bind in four different ways; each of these has two stable relative orientations, so this system has a total of eight meta-stable bound states. However, as they are all identical, many of these eight states are indistinguishable from each other and can all be collapsed into two functional states, A and B. This is depicted graphically in Fig. 5a. Nonetheless, note each of these meta-stable states corresponds to a different relative position and orientation between the molecules. We parametrize the MSM/RD scheme with the same setup as in the protein-protein system example, see SI Appendix B.

In Fig. 5, we compare MSM/RD results against the MD benchmark. We calculate FPTs for both the MD benchmark and the MSM/RD simulations in equal conditions. In Fig. 5b, we show the binding rates as a function of concentration, where each binding rate is calculated as the inverse of the mean first passage time (MFPT). The concentration is adjusted by changing the edge-length of the simulation box, starting at $30\,nm$ and increasing $5\,nm$ for each point. In Fig. 5c, we compare the FPTs distributions for several relevant transitions. Even when the original simulations to parametrize the scheme ran for only $30\,\mu s$, the MSM/RD scheme produces excellent results for transitions with higher MFPTs.

C. Multiparticle MSM/RD: formation of pentameric ring . We develop and implement the first multiparticle MSM/RD

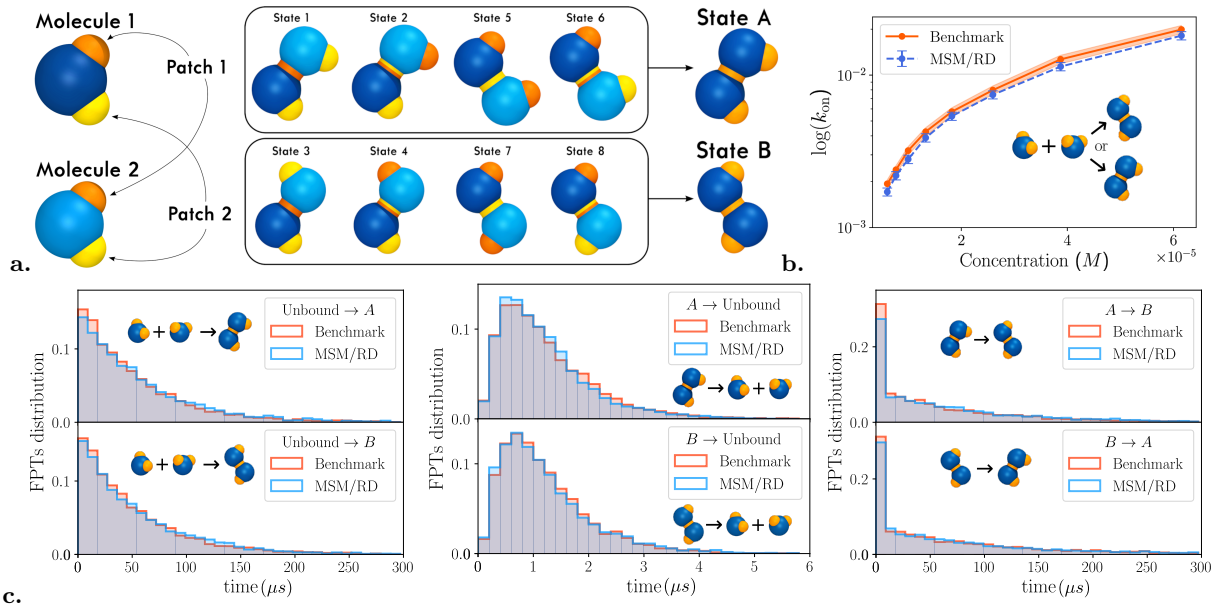


Fig. 5. Illustrations and results of the MSM/RD implementation for two identical interacting molecules with two interacting patches each and two stable angular configurations. **a**. The two molecules can bind in eight different ways (eight bound states). For illustration purposes, particle one is shown in dark blue and particle 2 in light blue; the first patch is shown in orange and the second one in yellow. All these states collapse into two bound states: A and B. **b**. Comparison of the on-rate, transition from unbound to either A or B state, for different molar concentrations. Each point was calculated as the inverse of the MFPT obtained from 5000 simulations; the error bars represent the standard deviation over 2000 bootstrapped samples. Note that in the generation of the MSM faster time-scales are neglected; therefore, it is expected that MSM/RD produces slightly slower results than the benchmark. **c.** Comparisons of the FPT distributions obtained with MSM/RD and the benchmark for six cases: from the unbound state to the two bound states and vice versa, and between the bound states. Each distribution was computed using 5000 simulations. These are shown next to each graph and they are all in μs. Note in the last two histograms there is a time-scale separation. This corresponds to the difference between direct transitions between the bound states and transitions that first unbound and later rebound in a different bound state.

Table 1. Comparison between the MD benchmark and MSM/RD of the rates of formation of pentameric rings for different concentrations. The rates were calculated as the inverse of the MFPTs averaged over 1000 simulations; the uncertainties represent the standard deviation over 100 bootstrapped samples.

Rate	Concentration	MD Benchmark	MSM/RD	% Error
k_{on} (ms^{-1})	$3.08 \cdot 10^{-4} M$	23.96 ± 0.44	22.67 ± 0.41	5.4%
	$1.94 \cdot 10^{-4} M$	16.16 ± 0.33	15.43 ± 0.31	4.5%
	$1.30 \cdot 10^{-4} M$	11.27 ± 0.23	11.72 ± 0.21	3.4%
	$9.11 \cdot 10^{-5} M$	8.42 ± 0.15	8.95 ± 0.16	6.3%
	$6.64 \cdot 10^{-5} M$	6.62 ± 0.13	6.99 ± 0.13	5.7%
	$4.99 \cdot 10^{-5} M$	5.50 ± 0.09	5.57 ± 0.08	3.6%

scheme to study the formation of pentameric ring molecules (inspired by (26)). The benchmark MD model is a modified version of the two-patch dimer model. It consists again of two identical molecules, each with two equally strong binding sites. Unlike the previous example, we only allow one meta-stable relative orientation per patch binding. We further increase the binding strength such that unbinding events are very rare and not observed in the timescales of interest. The particles can bind with each other forming chains, which eventually can close forming either trimeric, tetrameric or pentameric ring structures (Fig. 6a).

We parametrize the MSM/RD scheme with the same setup as in the protein-protein system example, see SI Appendix B. The multiparticle MSM/RD scheme requires modifications to the two-particle MSM/RD algorithm. These modifications are shown in SI Appendix C. We further need to estimate the diffusion coefficients of the multiparticle chains. We employ standard methods to estimate them (SI Appendix D).

In Fig. 6b, we compare MSM/RD results against the MD benchmark. We calculate FPTs for the formation of all the three ring molecules, using both the MD benchmark and the MSM/RD simulations in equal conditions: five particles with random positions and orientations placed in a simulation box of edge-length of 30nm with periodic boundaries. In Fig. 5c, we show the rate of formation of pentameric rings for different concentrations by changing the simulation box size. In Table 1, we show the exact values and relative errors of the rates plotted in Fig. 6c.

Note MSM/RD is not as good at approximating the formation of trimeric and tetrameric rings (Fig. 6b). This is due to MSM/RD modeling the particle-chains in steps 3 and 4 of Fig 6a as a fixed structure, while in the MD benchmark the chain is flexible, allowing for patches to get closer together, which increases the rate at which the ring is closed. This could be fixed by using a new MSM to describe the dynamics between the three or four particle chains and an additional particle. Nonetheless, note the rates of formation of pentameric rings are not affected by these problem since they are conditioned on not having trimeric or tetrameric rings forming beforehand. In its current formulation, MSM/RD multiparticle implementations are limited to non-crowded environments since only pair interactions are parametrized. It is important to take these issues into account when implementing MSM/RD applications.

V. Discussion

We presented a coarse-grained model of molecular kinetics based on hybrid switching diffusions. With this model, we

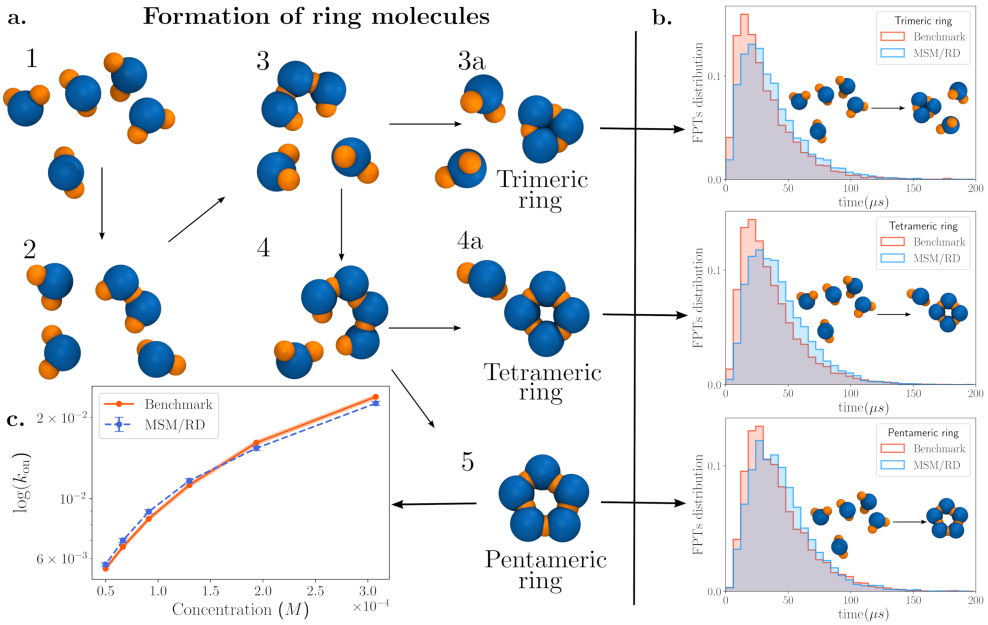


Fig. 6. Illustrations and multiparticle MSM/RD results for the formation of ring molecules. **a.** Diagram showing the formation of the trimeric, tetrameric and pentameric ring molecules. **b.** Comparisons of the FPT distributions obtained with multiparticle MSM/RD and the benchmark for the formation of the trimeric, tetrameric and pentemric ring molecules. The results were obtained from 5000 simulations for each case. **c.** Comparison of the rate at which a pentameric ring is generated for different molar concentrations. Each point was calculated as the inverse of the MFPT obtained from 1000 simulations; the error bars represent the standard deviation over 500 bootstrapped samples.

developed a robust framework for coupling Markov models of molecular kinetics with particle-based reaction diffusion (MSM/RD). Based on this framework, we derived one possible MSM/RD scheme by discretizing the underlying equation (Eq. 5), generalizing previous approaches (30). We implemented and verified it for three benchmark systems: the first two involve two protein-protein systems, while the third one is a multiparticle system to model the formation of pentameric molecules. We obtained an excellent agreement between the FPT distributions and reaction rates of relevant transitions.

The framework is well-suited to model protein-ligand binding in large domains and time-scales as in the previous work (30). Given enough data for the parametrization, it is also suited to model protein-protein dynamics since it incorporates arbitrary orientations, conformation switching and multiple binding sites. To parametrize the MSM/RD scheme for protein-protein systems, we would need the MD data of the two proteins interacting and individually, both in small simulation boxes. The interacting proteins data would serve to parametrize the scheme in the bound and transition regime, similarly to the works (68, 70, 74, 75) with the addition of the transition states, which might require a slightly larger box. The individual molecules data would serve to parametrize the scheme in the non-interacting regime. The resulting MSM/RD scheme could run simulations at much larger time- and length-scales than those allowed by MD.

The multiparticle implementation of MSM/RD has promising applications to the study of self-assembly of structures composed of several copies of the same molecule (or a small set of molecules), such as virus capsids (50) or soft matter self-assembly. This setting is ideal since we only need MD data of one pair (or a few pairs) of molecules in a small simulation box to parametrize an MSM/RD multiparticle simulation, which could potentially model the formation of the full capsid.

The main caveat of MSM/RD is that the parametrization requires a large amount of MD data, which is not yet possible to obtain for most systems of interest. However, given the increasing computational power, more and more systems will soon be within reach of MSM/RD. The scheme might also become less effective in the presence of long-ranged interactions, though it might be possible to incorporate them into the dynamics of the non-interacting-regime using coarse-grained potentials (63, 64). Finally, in its current form, the MSM/RD multiparticle implementation only takes into account pair interactions, and thus the scheme is not yet adequate for crowded multi-molecular environments.

Although application-dependent, one can expect MSM/RD to reduce computational cost by several orders of magnitude in comparison to MD. MD simulations propagate the position and velocity of every atom, which corresponds to several thousands of degrees of freedom in an average protein-protein simulation. MSM/RD only propagates two independent Brownian bodies together with an MSM. This corresponds to at most 14 degrees of freedom, 6 for the position/orientation and one for the MSM (per molecule). Finally, considering that MSM/RD can operate in larger domains with larger time steps, equivalent MD simulations would need to increase dramatically the number of solvent molecules yielding an exploding number of degrees of freedom, while still limited to small time steps.

Software. To enable reproducibility and implementation of this work, we developed the MSM/RD software package, a C++/python package. All the code and software developed for this work are open source and available under an MIT license in github.com/markovmodel/msmrd2 and Zenodo (55). The data used in this work was produced using the MSM/RD software.

ACKNOWLEDGMENTS. We acknowledge support by the European Commission (ERC CoG 772230), German Ministry for Education and Research (Berlin Institute for the Foundations of Learning and Data BIFOLD), Deutsche Forschungsgemeinschaft (SFB1114/C03 and TRR186/A12), the Berlin Mathematics research center Math+ (project AA1-6), and the Dutch Institute for Emergent Phenomena at the University of Amsterdam. M.J.R. thanks Hong Qian for helpful discussions over the course of this work. We also thank two anonymous reviewers that greatly improved the

presentation of this work.

Data Availability. The data and scripts to produce the plots in this work are available in Zenodo (65). The complete dataset that support the findings of this study are available from the corresponding author upon reasonable request.

References.

1. P Hänggi, P Talkner, M Borkovec, Reaction-rate theory: Fifty years after kramers. *Rev. Mod. Phys.* **62**, 251 (1990).
2. DT Gillespie, Stochastic simulation of chemical kinetics. *Annu. Rev. Phys. Chem.* **58**, 35–55 (2007).
3. D Shoup, A Szabo, Role of diffusion in ligand binding to macromolecules and cell-bound receptors. *Biophys. J.* **40**, 33–39 (1982).
4. SS Andrews, D Bray, Stochastic simulation of chemical reactions with spatial resolution and single molecule detail. *Phys. Biol.* **1**, 137 (2004).
5. N Agmon, A Szabo, Theory of reversible diffusion-influenced reactions. *J. Chem. Phys.* **92**, 5270–5284 (1990).
6. A Szabo, K Schulten, Z Schulten, First passage time approach to diffusion controlled reactions. *J. Chem. Phys.* **72**, 4350–4357 (1980).
7. IV Gopich, KM Solntsev, N Agmon, Excited-state reversible geminate reaction. i. two different lifetimes. *J. Chem. Phys* **110**, 2164–2174 (1999).
8. IV Gopich, A Szabo, Kinetics of reversible diffusion influenced reactions: the self-consistent relaxation time approximation. *J. Chem. Phys.* **117**, 507–517 (2002).
9. B Drawert, S Engblom, A Hellander, URDME: a modular framework for stochastic simulation of reaction-transport processes in complex geometries. *BMC Syst. Biol.* **6**, 76 (2012).
10. S Wils, E De Schutter, STEPS: Modeling and simulating complex reaction-diffusion systems with Python. *Front. Neuroinf.* **3**, art. no. 15 (2009).
11. K Takahashi, S Tănase-Nicola, PR Ten Wolde, Spatio-temporal correlations can drastically change the response of a mapk pathway. *Proc. Natl. Acad. Sci. U.S.A.* **107**, 2473–2478 (2010).
12. A Donev, et al., A first-passage kinetic monte carlo algorithm for complex diffusion–reaction systems. *J. Comput. Phys.* **229**, 3214–3236 (2010).
13. A Szabo, Theory of diffusion-influenced fluorescence quenching. *J. Phys. Chem.* **93**, 6929–6939 (1989).
14. MJ del Razo, W Pan, H Qian, G Lin, Fluorescence correlation spectroscopy and nonlinear stochastic reaction–diffusion. *The J. Phys. Chem. B* **118**, 7037–7046 (2014).
15. JS van Zon, PR ten Wolde, Green's-function reaction dynamics: a particle-based approach for simulating biochemical networks in time and space. *J. Chem. Phys.* **123**, 234910 (2005).
16. MJ del Razo, H Qian, A discrete stochastic formulation for reversible bimolecular reactions via diffusion encounter. *Commun. Math. Sci.* **14**, 1741–1772 (2016).
17. J Keizer, Nonequilibrium statistical thermodynamics and the effect of diffusion on chemical reaction rates. *The J. Phys. Chem.* **86**, 5052–5067 (1982).
18. J Keizer, Theory of rapid bimolecular reactions in solution and membranes. *Accounts Chem. Res.* **18**, 235–241 (1985).
19. J Keizer, Diffusion effects on rapid bimolecular chemical reactions. *Chem. Rev.* **87**, 167–180 (1987).
20. DF Anderson, TG Kurtz, *Stochastic analysis of biochemical systems*. (Springer) Vol. 1, (2015).
21. DJ Higham, An algorithmic introduction to numerical simulation of stochastic differential equations. *SIAM review* **43**, 525–546 (2001).
22. X Mao, C Yuan, *Stochastic differential equations with Markovian switching*. (Imperial College Press), (2006).
23. G Yin, C Zhu, *Hybrid switching diffusions: properties and applications*. (Springer New York) Vol. 63, (2010).
24. NV Buchete, G Hummer, Coarse master equations for peptide folding dynamics. *J. Phys. Chem. B* **112**, 6057–6069 (2008).
25. BE Husic, VS Pande, Markov state models: From an art to a science. *J. Am. Chem. Soc.* **140**, 2386–2396 (2018).
26. HC Klein, US Schwarz, Studying protein assembly with reversible brownian dynamics of patchy particles. *J. Chem. Phys.* **140**, 05B612_1 (2014).
27. S Delong, F Balboa Usabiaga, A Donev, Brownian dynamics of confined rigid bodies. *J. Chem. Phys.* **143**, 144107 (2015).
28. A Vijaykumar, TE Ouldridge, PR ten Wolde, PG Bolhuis, Multiscale simulations of anisotropic particles combining molecular dynamics and green's function reaction dynamics. *J. Chem. Phys.* **146**, 114106 (2017).
29. DC Rapaport, Molecular dynamics simulation using quaternions. *J. Comput. Phys.* **60**, 306–314 (1985).
30. M Dibak, MJ del Razo, D De Sancho, C Schütte, F Noé, MSM/RD: Coupling markov state models of molecular kinetics with reaction-diffusion simulations. *J. Chem. Phys.* **148**, 214107 (2018).
31. P Leopardi, A partition of the unit sphere into regions of equal area and small diameter. *Electron. Trans. Numer. Anal.* **25**, 309–327 (2006).
32. RC Bernardi, MC Melo, K Schulten, Enhanced sampling techniques in molecular dynamics simulations of biological systems. *Biochim. Biophys. Acta, Gen. Subj.* **1850**, 872–877 (2015).
33. IV Gopich, A Szabo, Reversible stochastically gated diffusion-influenced reactions. *J. Phys. Chem. B* **120**, 8080–8089 (2016).
34. AV Popov, N Agmon, IV Gopich, A Szabo, Influence of diffusion on the kinetics of excited-state association–dissociation reactions: Comparison of theory and simulation. *J. Chem. Phys.* **120**, 6111–6116 (2004).
35. PC Bressloff, Stochastic switching in biology: from genotype to phenotype. *J. Phys. A: Math. Theor.* **50**, 133001 (2017).
36. PC Bressloff, JN Maclaurin, Stochastic hybrid systems in cellular neuroscience. *J. Math. Neurosci.* **8**, 1–71 (2018).
37. PC Bressloff, SD Lawley, Hybrid colored noise process with space-dependent switching rates. *Phys. Rev. E* **96**, 012129 (2017).
38. PC Bressloff, SD Lawley, Stochastically gated diffusion-limited reactions for a small target in a bounded domain. *Phys. Rev. E* **92**, 062117 (2015).
39. PC Bressloff, SD Lawley, P Murphy, Protein concentration gradients and switching diffusions. *Phys. Rev. E* **99**, 032409 (2019).
40. M Hoffmann, C Fröhner, F Noé, Readdy 2: Fast and flexible software framework for interacting-particle reaction dynamics. *PLoS Comput. Biol.* **15**, e1006830 (2019).
41. MJ del Razo, H Qian, F Noé, Grand canonical diffusion-influenced reactions: A stochastic theory with applications to multiscale reaction-diffusion simulations. *The J. Chem. Phys.* **149**, 044102 (2018).
42. M Dibak, C Fröhner, F Noé, F Höfling, Diffusion-influenced reaction rates in the presence of pair interactions. *The J. chemical physics* **151**, 164105 (2019).
43. C Fröhner, F Noé, Reversible interacting-particle reaction dynamics. *The J. Phys. Chem. B* **122**, 11240–11250 (2018).
44. Z Schuss, A Singer, D Holcman, The narrow escape problem for diffusion in cellular microdomains. *Proc. Natl. Acad. Sci.* **104**, 16098–16103 (2007).
45. A Szabo, D Shoup, SH Northrup, JA McCammon, Stochastically gated diffusion-influenced reactions. *J. Chem. Phys.* **77**, 4484–4493 (1982).
46. H Wu, A Mardt, L Pasquali, F Noe, Deep generative markov state models in *Adv. Neural Inf. Process. Syst.* pp. 3975–3984 (2018).
47. M Linke, J Köfinger, G Hummer, Fully anisotropic rotational diffusion tensor from molecular dynamics simulations. *J. Phys. Chem. B* **122**, 5630–5639 (2018).
48. JT Bullerjahn, S von Bülow, G Hummer, Optimal estimates of self-diffusion coefficients from molecular dynamics simulations. *J. Chem. Phys.* **153**, 024116 (2020).
49. H Qian, MP Sheetz, EL Elson, Single particle tracking. analysis of diffusion and flow in two-dimensional systems. *Biophys. J.* **60**, 910–921 (1991).
50. A Arkhipov, PL Freddolino, K Schulten, Stability and dynamics of virus capsids described by coarse-grained modeling. *Structure* **14**, 1767–1777 (2006).
51. M Kostré, C Schütte, F Noé, MJ del Razo, Coupling particle-based reaction-diffusion simulations with reservoirs mediated by reaction-diffusion pdes. *arXiv preprint arXiv:2006.00003* - (2020).
52. AC Newton, J Groenewold, WK Kegel, PG Bolhuis, Rotational diffusion affects the dynamical self-assembly pathways of patchy particles. *Proc. Natl. Acad. Sci. U.S.A.* **112**, 15308–15313 (2015).
53. A Vijaykumar, PG Bolhuis, PR ten Wolde, Combining molecular dynamics with mesoscopic green's function reaction dynamics simulations. *J. Chem. Phys.* **143**, 214102 (2015).
54. J Schluttig, D Alamanova, V Helms, US Schwarz, Dynamics of protein-protein encounter: A langevin equation approach with reaction patches. *J. Chem. Phys.* **129**, 10B616 (2008).
55. MJ del Razo, M Dibak, C Schütte, F Noé, MSM/RD software (2021) http://dx.doi.org/10.5281/zenodo.4596416.
56. BR Jagger, SE Kochanek, S Haldar, RE Amaro, AJ Mulholland, Multiscale simulation approaches to modeling drug–protein binding. *Curr. Opin. Struct. Biol.* **61**, 213–221 (2020).
57. LW Votapka, BR Jagger, AL Heyneman, RE Amaro, SEEKR: simulation enabled estimation of kinetic rates, a computational tool to estimate molecular kinetics and its application to trypsin–benzamidine binding. *J. Phys. Chem. B* **121**, 3597–3606 (2017).
58. BR Jagger, CT Lee, RE Amaro, Quantitative ranking of ligand binding kinetics with a multiscale milestoning simulation approach. *J. Phys. Chem. Lett.* **9**, 4941–4948 (2018).
59. W Lim, B Mayer, T Pawson, *Cell signaling*. (Taylor & Francis), (2014).
60. RA Bradshaw, EA Dennis, *Handbook of cell signaling*. (Academic press), (2009).
61. JT Hancock, *Cell signalling*. (Oxford University Press), (2017).
62. T Hempel, et al., Independent markov decomposition: Towards modeling kinetics of biomolecular complexes. *Proc. Natl. Acad. Sci. U.S.A.* **118** (2021).
63. A Davtyan, et al., Awsem-md: protein structure prediction using coarse-grained physical potentials and bioinformatically based local structure biasing. *J. Phys. Chem. B* **116**, 8494–8503 (2012).
64. J Wang, et al., Multi-body effects in a coarse-grained protein force field. *J. Chem. Phys.* **154**, 164113 (2021).
65. MJ del Razo, M Dibak, C Schütte, F Noé, MSM/RD generated data/plots (2021) http://dx.doi.org/10.5281/zenodo.5236640.
66. A Mardt, L Pasquali, H Wu, F Noé, VAMPnets for deep learning of molecular kinetics. *Nat. Commun.* **9**, 5 (2018).
67. JD Chodera, F Noé, Markov state models of biomolecular conformational dynamics. *Curr. Opin. Struc. Biol.* **25**, 135–144 (2014).
68. N Plattner, S Doerr, GD Fabritiis, F Noé, Complete protein–protein association kinetics in atomic detail revealed by molecular dynamics simulations and markov modelling. *Nat. Chem.* **9**, 1005–1011 (2017).
69. S Doerr, MJ Harvey, F Noé, GD Fabritiis, HTMD: High-Throughput Molecular Dynamics for Molecular Discovery. *J. Chem. Theory Comput.* **12**, 1845–1852 (2016).
70. N Plattner, F Noé, Protein conformational plasticity and complex ligand binding kinetics explored by atomistic simulations and markov models. *Nat. Commun.* **6**, 7653 (2015).
71. GR Bowman, VS Pande, F Noé, eds., *An Introduction to Markov State Models and Their Application to Long Timescale Molecular Simulation*., Advances in Experimental Medicine and Biology. (Springer Heidelberg) Vol. 797, (2014).
72. F Noé, C Schütte, E Vanden-Eijnden, L Reich, TR Weikl, Constructing the full ensemble of folding pathways from short off-equilibrium simulations. *Proc. Natl. Acad. Sci. USA* **106**, 19011–19016 (2009).
73. JH Prinz, et al., Markov models of molecular kinetics: Generation and validation. *J. Chem. Phys.* **134**, 174105 (2011).
74. I Buch, T Giorgino, G De Fabritiis, Complete reconstruction of an enzyme-inhibitor binding process by molecular dynamics simulations. *Proc. Natl. Acad. Sci. USA* **108**, 10184–10189 (2011).

75. DA Silva, GR Bowman, A Sosa-Peinado, X Huang, A role for both conformational selection and induced fit in ligand binding by the lao protein. *PLoS Comput. Biol.* **7**, e1002054 (2011).
76. JSV Zon, PR ten Wolde, Simulating biochemical networks at the particle level in time and space: Green's function reaction dynamics. *Phys. Rev. Lett.* **94**, 128103 (2005).
77. P Mereghetti, D Kokh, JA McCammon, R Wade, Diffusion and association processes in biological systems: theory, computation and experiment. *BMC biophysics* **4**, 2 (2011).
78. J Schöneberg, A Ullrich, F Noé, Simulation tools for particle-based reaction-diffusion dynamics in continuous space. *BMC Biophys.* **7**, 11 (2014).

Supplementary information: Multiscale molecular kinetics by coupling Markov state models and reaction-diffusion dynamics.

Mauricio J. del Razo, Manuel Dibak, Christof Schütte and Frank Noé

A. Molecular kinetics as hybrid switching diffusion processes

A.1. A first derivation of a hybrid switching diffusion process . We first introduce the hybrid switching diffusion model for a simple scenario, which can be easily generalized to more complex cases. Consider one macromolecule A with N atoms and assume the molecule follows overdamped Langevin dynamics, the corresponding stochastic differential equation (SDE) is

$$dq(t) = -\nabla U(q)dt + \Sigma dW(t) \qquad \text{[S1]}$$

with $q(t) = [q_1, \cdots, q_N]$ and q_i the three-dimensional positions of the i^{th} atom, $U(q(t))$ the potential function of the interactions, Σ a matrix related to the diffusion tensor and $W(t)$ is an $3N$ dimensional vector of standard Brownian motions. This equation describes the trajectories of the molecule's atoms. Alternatively, we can focus on the dynamics of the corresponding probability density function. This is given in terms of the Fokker-Planck equation

$$\begin{aligned} &\partial_t f(q,t) = \mathcal{L} f(q,t) \\ \text{with} \qquad &\mathcal{L} f(q) = \sum_{i,j=1}^{d} \left[\partial^2_{q_i q_j}(D_{ij} f(q))\right] + \nabla U(q)\cdot\nabla f(q) + \\ &\qquad \nabla^2 U(q) f(q), \end{aligned} \qquad \text{[S2]}$$

where D_{ij} are the entries of the diffusion tensor $D = \frac{1}{2}\Sigma\Sigma^{\mathrm{T}}$. The operator $\mathcal{L}$ is called the infinitesimal generator. If Σ is a diagonal matrix (uncorrelated Brownian motions) with the same constant value σ in each entry, we recover the well-known Smoluchowski model $\mathcal{L} f = D\nabla^2 f + \nabla\cdot(f\nabla U)$, with $D = \sigma^2/2$. Consider the molecule as a rigid body with its center of mass given by $r(t)$, and its orientation given by the quaternion θ. To better analyze the molecule's configurations, we change to the frame of reference of the molecule:

$$\tilde{q}_i(t) = R_\theta^{-1}[q_i(t) - r(t)] \qquad \Rightarrow \qquad q_i(t) = r(t) + R_\theta \tilde{q}_i(t), \qquad \text{[S3]}$$

where $r(t) = \sum_{i=1}^{N} q_i(t)/N$; R_θ is a rotation matrix corresponding to a rotation by the quaternion θ; R_θ^{-1} is the inverse rotation matrix; and $\tilde{q}(t) = [\tilde{q}_i(t), \dots \tilde{q}_N(t)]$ are the coordinates of the atoms in the molecules's frame of reference. As r and θ are both functions of q, we could use Ito's formula in conjunction with Eq. (S1) to derive SDEs for r and θ. We could also use the relations just derived to obtain SDEs for the atom variables in the new coordinates $\tilde{q}$. Although this can be written explicitly, it is more convenient for our analysis to write directly the Fokker-Planck equation in the new variables. As the Fokker-Planck equation is linear, we can split the operator $\mathcal{L}$ into two parts: $\mathcal{L}_x$ the diffusion and drift operating in the molecule's position and orientation coordinates, $x = (r, \theta)$, and $\mathcal{L}_{\tilde{q}}$ operating on the atoms positions $\tilde{q}$ in the molecule's frame of reference,

$$\partial_t f(x,\tilde{q},t) = \underbrace{\mathcal{L}_x f(x,\tilde{q},t)}_{\substack{\text{Molecule translation} \\ \text{and rotation}}} + \underbrace{\mathcal{L}_{\tilde{q}} f(x,\tilde{q},t)}_{\substack{\text{Atoms diffusion in} \\ \text{molecule's frame of ref.}}} . \qquad \text{[S4]}$$

Note it seems we increased the dimensionality of our problem by six when adding r and θ. However, we can simply get rid of two random coordinates in vector $\tilde{q}(t)$ and recover them through the relations in Eqs. (S3). This issue will not be relevant since we will apply dimensionality reduction techniques.

A.1.1. Propagators. It is sometimes convenient to express the last equation in terms of the propagator. To do so, we integrate Eq. S4 from t to $t+\tau$,

$$f(x,\tilde{q},t+\tau) = f(x,\tilde{q},t) + \int_t^{t+\tau} \mathcal{L}_x f(x,\tilde{q},s)ds + \int_t^{t+\tau} \mathcal{L}_{\tilde{q}} f(x,\tilde{q},s)ds.$$

This defines the propagator operators $\mathcal{P}_x$ for the molecule's translational and rotational diffusion and $\mathcal{P}_{\tilde{q}}$ for the diffusion of the atoms in the new coordinates, both of which depend on the lag-time τ chosen. The equation is then

$$f(x,\tilde{q},t+\tau) = f(x,\tilde{q},t) + \mathcal{P}_x f(x,\tilde{q},t) + \mathcal{P}_{\tilde{q}} f(x,\tilde{q},t). \qquad \text{[S5]}$$

A.1.2. Galerkin discretization. We call Ω the portion of the phase space spanned by the coordinates $\tilde{q}(t)$. In this section, we use methods similar to those presented in (17) to discretize Ω into a discrete state space. As the coordinates $\tilde{q}(t)$ are aligned with the molecule, we will observe meta-stable regions in the Ω phase space corresponding to the different stable structures or conformations of the molecule. We assume there are M meta-stable regions denoted by $[s_1, \cdots, s_M]$; each of these regions defines a state or conformation of the molecule $1, \dots, M$. We then define indicator functions on these regions/states

$$\chi_i(\tilde{q}) = \begin{cases} 1 & \text{if} \quad \tilde{q} \in s_i, \\ 0 & \text{else.} \end{cases}$$

We discretize the continuous operator $\mathcal{P}_{\tilde{q}}$ into a discrete operator by doing a Galerkin discretization with these indicator functions as basis functions. This is achieved by multiplying Eq. (S5) by $\chi_i(x)$ and integrating over Ω

$$f_i(x,t+\tau) = f_i(x,t) + \int_\Omega \chi_i(\tilde{q})\mathcal{P}_x f(x,\tilde{q},t)d\tilde{q} + \int_\Omega \chi_i(\tilde{q})\mathcal{P}_{\tilde{q}} f(x,\tilde{q},t)d\tilde{q}, \qquad \text{[S6]}$$

where we used that

$$f_i(x,t) = \int_\Omega \chi_i(\tilde{q}) f(x,\tilde{q},t)d\tilde{q}$$

is the probability of being in the meta-stable region χ_i at a given time. The operator $\mathcal{P}_x$ in the first integral corresponds to the diffusion propagator for the translational and rotational motion of the molecule, and we expect it to behave differently for different conformations of the molecule. In general, $\mathcal{P}_x$ depends on $\tilde{q}$ through the potential (see Eq. (S2)), so it cannot simply exchange order with the integration. However, if the molecule remains on the i^{th}meta-stable region, we do not expected any significant change on $\mathcal{P}_x$, so we can approximate it by $\mathcal{P}_x^i$, which depends on the conformation i but not on $\tilde{q}$. Thus, we can approximate the first integral by

$$\int_\Omega \chi_i(\tilde{q})\mathcal{P}_x f(x,\tilde{q},t)d\tilde{q} \approx \mathcal{P}_x^i f_i(x,t),$$

We still need to further simplify the last term of Eq. S6. To do so, we focus to the eigenfunctions of $\mathcal{P}_{\tilde{q}}$,

$$\mathcal{P}_{\tilde{q}}\psi = \lambda\psi.$$

We then expand $f(x,\tilde{q},t)$ in these eigenfunctions, $f = \sum_{j=1}^{\infty}\langle f,\psi_j\rangle\psi_j$, and apply $\mathcal{P}_{\tilde{q}}$

$$\mathcal{P}_{\tilde{q}} f = \sum_{j=0}^{\infty} \lambda_j \langle f,\psi_j\rangle\psi_j.$$

As we are interested in slow processes, such as conformation switching, we focus on larger time-scales. This means truncating this sum to only include the K slowest processes, $\sum_{j=0}^{K}\lambda_j\langle f,\psi_j\rangle\psi_j$, where we assumed the indexing of the eigenvalues/eigenfunctions to follow $\lambda_0 \geq \lambda_1 \geq \cdots \geq \lambda_K$. Then the last term of Eq. S6 is simply approximated by

$$\int_\Gamma \chi_i(\tilde{q})\mathcal{P}_{\tilde{q}}f(x,\tilde{q},t)d\tilde{q} \approx \sum_{j=1}^{K}\lambda_j\langle f,\psi_j\rangle\psi_j^i V_i$$

where $\psi_j^i = \frac{1}{V_i}\int_\Omega \chi_i(\tilde{q})\psi_j d\tilde{q}$ is the average value of the j^{th} eigenfunction over the i^{th} state, and V_i is the volume of the i^{th} state in the phase space Ω. The inner product integral can be then approximated by piecewise constant values along the states, $\langle f,\psi_j\rangle = \int_\Omega f(x,\tilde{q},t)\psi_j(\tilde{q})d\tilde{q} \approx \sum_{k=1}^{M} f_k(x,t)\psi_j^k$, so the last term is simply

$$\int_\Gamma \chi_i(\tilde{q})\mathcal{P}_{\tilde{q}}f(x,\tilde{q},t)d\tilde{q} \approx \sum_{k=1}^{M} f_k(x,t)\underbrace{V_i\sum_{j=1}^{K}\lambda_j\psi_j^k\psi_j^i}_{\alpha_{ik}},$$

Consequently, Eq. S6 is simplified to

$$f_i(x,t+\tau) = f_i(x,t) + \mathcal{P}_x^i f_i(x,t) + \sum_{k=1}^{M}\alpha_{ik}f_k(x,t).$$

We refer to this as the discrete-time hybrid switching diffusion model, which can also be written in its vector form

$$\bar{f}(x,t+\tau) = \bar{f}(x,t) + \mathcal{P}_x\bar{f}(x,t) + \mathbb{P}\bar{f}(x,t), \qquad [S7]$$

where $\bar{f}(x,t) = [f_1(x,t),\cdots,f_M(x,t)]$ is a vector with functions as entries, and it corresponds to a partially discrete approximation to the probability density f from Eq. S4. Each function in the vector $f_i(x,t)$ corresponds to the probability density of observing the molecule in conformation i at position and orientation x at time t. The term $\mathcal{P}_x\bar{f}(x,t) = [\mathcal{P}_x^1 f_1(x,t),\cdots,\mathcal{P}_x^M f_M(x,t)]$ is the vector of diffusion propagators, each corresponding to a different conformation. The last term is a discrete-time MSM, where $\mathbb{P}$ is an $M\times M$ transition probability matrix with entries α_{ik} representing the transition probabilities between the states or conformations. As probability must be conserved, the columns of the transition matrix $\mathbb{P}$ must sum to one, $\sum_{i=1}^{M}\alpha_{ik} = 1$. This can be achieved by renormalizing the rates α_{ik} by multiplying them by a renormalization factor w_i, such that the condition that needs to be satisfied is $\sum_{i=1}^{M} w_i\alpha_{ik} = 1$. This yields a system of M unknowns with M equations, so we can solve for every w_i. This renormalization is valid because it corresponds to multiplying each eigenfunction by a constant factor, which remains an eigenfunction.

In practice, we extract the rates in $\mathbb{P}$ from data using the methodology from (17) and the core MSMs approach from (15). We should also point out it is possible to derive conservative discretizations by smartly choosing non-constant basis functions $\chi(\tilde{q})$, such as in the discontinuous Galerkin methods.

A.1.3. The hybrid switching diffusion model. The model we derived in Eq. S7 can be framed in a continuous time context. If we divide the equation S7 by τ and take the limit $\tau\to 0$, we obtain an equation similar to the original Fokker-Planck equation (Eq. S4),

$$\partial_t\bar{f}(x,t) = \underbrace{\mathcal{D}\bar{f}(x,t)}_{\substack{\text{Molecule translation}\\ \text{and rotation}}} + \underbrace{\mathbb{Q}\bar{f}(x,t)}_{\substack{\text{Continuous-time}\\ \text{MSM}}}, \qquad [S8]$$

where $\mathbb{Q}$ is now a transition-rate matrix modeling the molecule's conformation changes. The molecule's translational and rotational diffusion is modeled by $\mathcal{D}\bar{f} = [\mathcal{D}_1 f_1,\cdots,\mathcal{D}_M f_M]$. These entries are obtained as the limit, $\mathcal{D}_i f_i = \lim_{\tau\to 0}\mathcal{P}_x f_i/\tau$. We refer to this model simply as the hybrid switching diffusion model. The main differences with respect to Eq. S4 are that here the phase space spanned by q was discretized into meta-stable regions and that the dynamics of fast processes have been filtered out.

Alternatively one could also write the following SDE to describe the individual stochastic trajectories, whose ensemble distribution dynamics are governed by Eq. 1

$$dX(t) = \mu(X(t),\eta(t),t)dt + \sigma(X(t),\eta(t),t)dW(t), \qquad [S9]$$

where $X(t)$ corresponds to the postion and orientation of the molecule, the drift μ and the diffusion σ depend on the form of the diffusion operator $\mathcal{D}$, as well as on the current conformation of the molecule $\eta(t)$,with $\eta(t)$ only accepting discrete values. The random conformation at a given time for one trajectory can be computed using a Gillespie-type algorithm based on the rates in matrix $\mathbb{Q}$.

Equation S8 is an example of a hybrid switching diffusion process. This is a well-defined stochastic process, and it has been thoroughly studied in (1, 2). These hybrid switching diffusions (2) models are also known in the mathematics community as diffusion processes with Markovian switching (1) or coupled diffusion models. They are called 'hybrid' due to the coexistence of continuous dynamics and discrete events in the same process.

The switching diffusion model can be formulated using discrete time (Eq. S7) or continuous time (Eq. S8), depending of which formulation is more convenient for the corresponding application. The translational and rotational diffusion of the molecule is modeled by either $\mathcal{P}_x\bar{f}$ or $\mathcal{D}\bar{f}$, while the switching between different states or conformations of the molecule is modeled by a discrete-time or continuous-time MSM, $\mathbb{P}$ and $\mathbb{Q}$, respectively.

A.2. Hybrid switching diffusion for one molecule . In a more realistic setting, we need to provide a more robust model for the dynamics. Consider the dynamics of one molecule A, with N atoms. Assume molecule A has M conformations. The position and momentum of the N atoms is given by $q(t)$ and $p(t)$, respectively. Analogously to the previous example, we assume the dynamics of the stochastic dynamical system are governed by the Langevin equation,

$$\begin{aligned} dq(t) =& p(t)dt,\\ dp(t) =& -\nabla_q U(q(t))dt - \Gamma p(t)dt + \Sigma dW(t), \end{aligned} \qquad [S10]$$

where to simplify notation, we assumed the mass of all atoms to be one; $U(q(t))$ is the interaction potential; Γ is a diagonal matrix with the damping coefficients γ_i along the diagonal; Σ is a matrix that correlates the noise vector, and $W(t)$ is a vector of standard Brownian motions. The corresponding Fokker-Planck equation for the probabilistic dynamics in phase space is then given by

$$\partial_t f(q,p,t) = \mathcal{L}_A f(q,p,t) \qquad [S11]$$

where $f(q(t),p(t),t)$ is the probability density function of the system as a function of $(q(t),p(t),t)$; the Langevin operator is $L_A = [\nabla_p\cdot D\nabla - p\cdot\nabla_q + \nabla_q U(q)\cdot\nabla_p + \gamma p\cdot\nabla_p + \mathrm{tr}(\Gamma)]$, $D = \frac{1}{2}\Sigma\Sigma^{\mathrm{T}}$, $\mathrm{tr}(\Gamma)$ is the trace of Γ. The operators ∇_q, ∇_p are the gradient operators with respect to the position and momentum coordinates, respectively. Note if the noise is uncorrelated, Σ and D are diagonal matrices with $\sigma_{ii} = \sqrt{2k_BT\gamma_i}$ and $D_{ii} = \sigma_{ii}^2/2$, along the diagonal.

Following Section A.1 and Eq. S3, we change again the frame of reference to the center of mass of A, $r_A = \frac{1}{N}\sum_{i=1}^{N} q_i(t)$, and we rotate the frame by θ_A^{-1} to align it to the molecule. Similarly, we need to transform the momentum coordinates,

$$\tilde{p}_i(t) = R_\theta^{-1}p_i(t), \qquad p_A(t) = \frac{1}{N}\sum_{i=1}^{N} p_i(t),$$

where p_A correspond to the velocity of the center of mass. The molecule's angular momentum in the center of mass reference is given by ω_A, which is a function p. Note the translation to the center of mass is invariant for the velocities. We can again derive SDEs for r_A, p_A, θ_A and ω_A and for all the atoms variables in the new coordinates $\tilde{q}_i(t)$ and $\tilde{p}_i(t)$. The Fokker-Planck equation can be now conveniently separated into an operator acting on the molecule's position, velocity, orientation and angular momentum $z = (r_A,p_A,\theta_A,\omega_A)$, and another operator acting on the individual atoms position and momentum,q and p, in the molecule's reference system,

$$\partial_t f(z,\tilde{q},\tilde{p},t) = \underbrace{\mathcal{L}_D f(z,\tilde{q},\tilde{p},t)}_{\substack{\text{Molecule translation}\\ \text{and rotation}}} + \underbrace{\mathcal{L}_{qp} f(z,\tilde{q},\tilde{p},t)}_{\substack{\text{Atoms diffusion in}\\ \text{molecule's frame of ref.}}} . \quad [S12]$$

Following the same methodology as in Appendix A.1, we obtain the hybrid switching diffusion model for one molecule,

$$\partial_t \bar{f}(z,t) = \underbrace{D_A \bar{f}(z,t)}_{\substack{\text{Molecule translation}\\ \text{and rotation}}} + \underbrace{Q_A \bar{f}(z,t)}_{\substack{\text{Continuous-time}\\ \text{MSM}}} .$$

where $\bar{f}(z,t) = [f_1(z,t), \cdots, f_M(z,t)]$. In the cases where the time-scales we are interested in are larger than the autocorrelation decay times of $p_A$and ω_A, the first operator can be approximated by overdamped operators for the diffusion and rotation, $D_A \approx \mathcal{D}_A$, the momentum coordinates become irrelevant, and the transition rate matrix Q_A is projected into the corresponding space resulting in $\mathbb{Q}_A$. This simplifies the system to

$$\partial_t \bar{f}(x,t) = \mathcal{D}_A \bar{f}(x,t) + \mathbb{Q}_A \bar{f}(x,t), \quad [S13]$$

where $x = (r_A, \theta_A)$. This equation is exactly of the same form as Eq. S8. Note if the time-scales of interest are even larger than the time-scales for conformational changes described by Q_A, the MSM becomes irrelevant, the vector $\bar{f}(x,t)$ has only one component, and the diffusion properties of the different conformations are averaged out by $\mathcal{D}_A$, recovering the Fokker-Planck equation for one diffusing and rotating particle. Although not yet explored, more complex derivations formally taking into account the solvent could lead to interesting models with memory kernels (4, 5).

A.3. Hybrid switching diffusion for two interacting molecules . Consider the dynamics of two molecules A and B, each one with $N_A$and N_B atoms, respectively. Assume molecule A has M_A conformations and B has M_B conformations, and they can bound in M_C different meta-stable configurations. The position and momentum of every atom is given by $q(t) = [q_A(t), q_B(t)]$ and $p(t) = [p_A(t), p_B(t)]$ ($q_X(t)$ and $p_X(t)$ denote the positions and momentum of all the atoms in molecule X). Analogous to Appendix A.2, we assume all the masses are one and that the dynamics of the stochastic dynamical system are governed by the Langevin equation

$$\begin{aligned} dq(t) &= p(t)dt, \\ dp(t) &= -\nabla_q U(q(t))dt - \Gamma p(t)dt + \Sigma dW(t) \end{aligned}$$

The corresponding Fokker-Planck equation is given by,

$$\begin{aligned} \partial_t f(q,p,t) &= L_{AB} f(q,p,t) \quad [S14] \\ L_{AB} &= \frac{1}{2}\nabla_p \cdot D\nabla_p - p\cdot\nabla_q + \nabla_q U(q)\cdot\nabla_p \\ &\quad + \gamma p\cdot\nabla_p + \mathrm{tr}(\Gamma) \end{aligned}$$

where $f(q(t),p(t),t)$ is the probability density of the system as a function of $(q(t),p(t),t)$, $D = \frac{1}{2}\Sigma\Sigma^{\mathrm{T}}$, and L_{AB} is the infinitesimal generator of the process. The potential function can be rewritten as a sum of the independent potentials corresponding to each molecule plus an interaction term

$$U(q) = U_A(q_A) + U_B(q_B) + \Phi(r_{AB})U_{AB}(q_A, q_B),$$

where $r_{AB} = |r_B - r_A|$ is the distance between the two molecules, with r_A and r_B the centers of mass of A and B. The function $\Phi(r_{AB})$ varies between 0 and 1 to weight how strong is the interaction as a function of r_{AB}, so when the molecules are close ($r_{AB} \ll 1$), $\Phi(r_{AB}) = 1$ and when they are far apart ($r_{AB} \gg 1$), $\Phi(r_{AB}) = 0$. This divides our phase space in three regimes: the non-interacting regime ($\Phi(r_{AB}) = 0$), the transition regime ($0 < \Phi(r_{AB}) < 1$), and the bound regime ($\Phi(r_{AB}) = 1$).

A.3.1. Non-interacting regime. In this regime $\Phi(r_{AB}) = 0$, so we only have the first two terms in the potential. Furthermore, when r_{AB} is large, the two molecules dynamics are independent, so the joint probability can be separated as the product of the probability densities corresponding to each molecule $f_{AB}(q,p,t) = f_A(q_A,p_A,t)f_B(q_B,p_B,t)$. Taking this into consideration we can rewrite each term of Eq. S14 as a term acting on the coordinates (q_A,p_A) or (q_B,p_B),

$$\begin{aligned} \partial_t(f_A f_B) = \Big[&\frac{1}{2}\nabla_{p_A}\cdot D_A\nabla_{p_A} - p_A\cdot\nabla_{q_A} + \nabla_{q_A}V_A(q_A)\cdot\nabla_{p_A} \\ &+\gamma p_A\cdot\nabla_{p_A} + \mathrm{tr}(\Gamma_A) + \frac{1}{2}\nabla_{p_B}\cdot D_B\nabla_{p_B} - p_B\cdot\nabla_{q_B} \\ &+\nabla_{q_B}V_B(q_B)\cdot\nabla_{p_B} + \gamma p_B\cdot\nabla_{p_B} + \mathrm{tr}(\Gamma_B)\Big] f_A f_B, \end{aligned}$$

where D_X is a block matrix of D corresponding to the molecule X, Γ_x is the block matrix of Γ corresponding to X, and we omitted variable dependencies to ease notation. Notice that $\mathrm{tr}(\Gamma) = \mathrm{tr}(\Gamma_A) + \mathrm{tr}(\Gamma_B)$. The left hand side can be simply expanded as $f_A\partial_t f_B + f_B\partial_t f_A$, where ∂t denotes partial derivative with respect to t, and we can divide the whole equation by $f_A f_B$ to obtain,

$$\begin{aligned} &\frac{\partial_t f_A}{f_A} + \frac{\partial_t f_B}{f_B} = \\ &\frac{1}{f_A}\Big[\frac{1}{2}\nabla_{p_A}\cdot D_A\nabla_{p_A} - p_A\cdot\nabla_{q_A} + \nabla_{q_A}V_A(q_A)\cdot\nabla_{p_A} \\ &\qquad +\gamma p_A\cdot\nabla_{p_A} + \mathrm{tr}(\Gamma_A)\Big] f_A + \\ &\frac{1}{f_B}\Big[\frac{1}{2}\nabla_{p_B}\cdot D_B\nabla_{p_B} - p_B\cdot\nabla_{q_B} + \nabla_{q_B}V_B(q_B)\cdot\nabla_{p_B} \\ &\qquad +\gamma p_B\cdot\nabla_{p_B} + \mathrm{tr}(\Gamma_B)\Big] f_B. \end{aligned}$$

Note we have only functions of (q_A,p_A) or (q_B,p_B) and constants. We can move the terms such that the left hand side is only a function of (q_A,p_A) and the right hand side just a function of (q_B,p_B), such that for the equality to hold they must be equal to a constant. Considering these are equations that described probabilities, the only reasonable choice for this constant is zero, so

$$\begin{aligned} \partial_t f_A &= \Big[\frac{1}{2}\nabla_{p_A}\cdot D_A\nabla_{p_A} - p_A\cdot\nabla_{q_A} + \nabla_{q_A}V_A(q_A)\cdot\nabla_{p_A} \\ &\quad + \gamma p_A\cdot\nabla_{p_A} + \mathrm{tr}(\Gamma_A)\Big] f_A \\ \partial_t f_B &= \Big[\frac{1}{2}\nabla_{p_B}\cdot D_B\nabla_{p_B} - p_B\cdot\nabla_{q_B} + \nabla_{q_B}V_B(q_B)\cdot\nabla_{p_B} \\ &\quad + \gamma p_B\cdot\nabla_{p_B} + \mathrm{tr}(\Gamma_B)\Big] f_B, \end{aligned}$$

which is by definition the infinitesimal generator for the independent dynamics of each of the two individual molecules,

$$\begin{aligned} \partial_t f_A(q_A,p_A,t) &= \mathcal{L}_A f_A(q_A,p_A,t), \\ \partial_t f_B(q_B,p_B,t) &= \mathcal{L}_B f_B(q_B,p_B,t). \end{aligned} \quad [S15]$$

This further means that we have two independent Langevin equations for each molecule. Following the methodology from Appendix A.2 and assuming the diffusion dynamics are accurately approximated by overdamped Langevin dynamics, see Eq. S13, we can then write a hybrid switching diffusion model for each of the molecules

$$\begin{aligned} \partial_t \bar{f_A}(x_A,t) &= \mathcal{D}_A \bar{f_A}(x_A,t) + \mathbb{Q}_A \bar{f_A}(x_A,t), \\ \partial_t \bar{f_B}(x_B,t) &= \mathcal{D}_B \bar{f_B}(x_B,t) + \mathbb{Q}_B \bar{f_B}(x_B,t), \end{aligned} \quad [S16]$$

where $x_i = (r_i, \theta_i)$ is the position and orientation of molecule i. The vectors $\bar{f_A}$ and $\bar{f_B}$ have the dimensions of the individual conformations M_A and M_B, respectively. The transition rate matrices $\mathbb{Q}_A$ and $\mathbb{Q}_B$ have dimensions $M_A \times M_A$ and $M_B \times M_B$, respectively. Although at this point we can describe each molecule individually, it will be useful to show the state of the full system is simply given by the tensor product $\bar{f}_{AB} = \bar{f_A} \otimes \bar{f_B}$. Its solution is the tensor product of the individual solutions,

$$\bar{f}_{AB}(t) = e^{t\mathcal{D}_A} \otimes e^{t\mathcal{D}_B} \otimes e^{t(\mathbb{Q}_A \oplus \mathbb{Q}_B)} \bar{f}_0,$$

with $\bar{f}_0 = \bar{f_A}(0) \otimes \bar{f_B}(0)$. This way we can define the coupled diffusion coefficient as $e^{tD_{AB}} = e^{t\mathcal{D}_A} \otimes e^{t\mathcal{D}_B}$. This last equation describes the diffusion of the system in terms of the diffusion of the centers of mass and orientation of the two molecules, and it

describes its state in terms of the continuous-time MSM given by the transition rate matrix

$$\mathbb{Q}_{AB} = \mathbb{Q}_A \oplus \mathbb{Q}_B.$$

This type of sum is called the Kronecker sum. Note that in the case of the discontinuous-time hybrid switching diffusion model, the resulting MSM will simply be given by the tensor product of the transition matrices $\mathbb{P}_{AB} = \mathbb{P}_A \otimes \mathbb{P}_B$, since $\bar{f}_{AB}(t) = e^{t\mathcal{D}_A} \otimes e^{t\mathcal{D}_B} \otimes (\mathbb{P}_A \otimes \mathbb{P}_B)\, \bar{f}_0$.

A.3.2. Bound regime. In this case, as $\Phi(r_{AB}) = 1$, we are not able to uncouple Eq. S14 into the independent molecules dynamics, so we have no alternative but to describe the dynamics of the joint complex. Therefore we apply the same change of variables as in Appendix A.2 for the position and momentum of the joint complex, C. Following the same methodology as in Appendix A.2 and assuming the diffusion dynamics can be approximated by overdamped Langevin dynamics, we obtain the hybrid switching diffusion model for the two coupled molecules in the small separation regime,

$$\partial_t \bar{f}_C(x,t) == \underbrace{\mathcal{D}_C \bar{f}_C(x,t)}_{\substack{C \text{ translation} \\ \text{and rotation}}} + \underbrace{\mathbb{Q}_C \bar{f}_C(x,t)}_{\substack{\text{MSM for} \\ C \text{ complex}}}, \qquad \text{[S17]}$$

with $z = (r_C, \theta_C)$, corresponding to the C-complex center of mass position and orientation; and where $\bar{f}_C$ has the dimensions of all the possible bound configurations between the two molecules M_C, and $\mathbb{Q}_c$ has dimensions $M_C \times M_C$.

A.3.3. Transition regime. We would like to have a regime that allows us to transition between the non-interacting and bound regime from Eqs. S16 and S17, respectively. The interactions are encoded in the transition rate matrix $\mathbb{Q}$ and should depend on the separation between the two molecules, $r_{AB} = |r_B - r_A|$, as well as in their relative orientation, $\theta_{AB} = \theta_B \theta_A^{-1}$. Therefore, the transition rate matrix $\mathbb{Q}(x_{AB})$ depends on $x_{AB} = (r_{AB}, \theta_{AB})$. In the non-interacting regime, Eq. S16 corresponds to $r_{AB} \gg 1$such that the dependence on x_{AB} is zero and $\mathbb{Q}(x_{AB}) \to \mathbb{Q}_A \oplus \mathbb{Q}_B$. In the bound regime, the dependence on x_{AB} is again lost, and all transitions are governed by $\mathbb{Q}_C$, unless there is a dissociation event. We thus need a transition regime, where the rates depend on x_{AB} and the system can transition from a dissociated state to a bound state and vice versa. This can be achieved by incorporating the two limiting models we just obtained into a larger switching diffusion process that can interact through the rate matrices $\mathbb{Q}_{AB\to C}$ and $\mathbb{Q}_{C\to AB}$. This can be done by writing the transition matrix $\mathbb{Q}$as a block matrix

$$\frac{\partial \bar{f}(x)}{\partial t} = \mathcal{D}\bar{f}(x) + \mathbb{Q}(x_{AB})\bar{f}(x),$$
$$\mathbb{Q}(x_{AB}) = \left(\begin{array}{c|c} \mathbb{Q}_{AB} & \mathbb{Q}_{C\to AB} \\ \hline \mathbb{Q}_{AB\to C} & \mathbb{Q}_C \end{array}\right),$$

where $\bar{f} = (\bar{f}_{AB}, \bar{f}_C)$, with $\bar{f}_{AB} = \bar{f}_A \otimes \bar{f}_B$ the vector of all the unbound states given by the tensor product of independent states of A and B, and $\bar{f}_C$ the vector of all the bound states of the $C-$complex. The diffusion term $\mathcal{D}\bar{f}(x)$ can in principle also depend on x_{AB}; however, it can be approximated by the combined diffusions of the two limiting cases $\mathcal{D}\bar{f} = [\mathcal{D}_{AB}\bar{f}_{AB}, \mathcal{D}_C \bar{f}_C]$ since the interactions are already encoded in $\mathbb{Q}$. Overall, $\bar{f}$ has dimension $M = M_A M_B + M_C$ and $\mathbb{Q}$ has dimensions $M \times M$. In the non-interacting regime $\mathbb{Q}_{AB} = \mathbb{Q}_A \oplus \mathbb{Q}_B$ and $\mathbb{Q}_{AB\to C} = 0$. In the transition regime, $\mathbb{Q}_{AB\to C} \neq 0$ and $\mathbb{Q}_{AB}$ has to change as well, both dependent on x_{AB}. The transition rate functions $\mathbb{Q}_{AB}$ together with the transition rate functions $\mathbb{Q}_{AB\to C}$ should always have their combined columns in $\mathbb{Q}$ sum to zero, for any given x_{AB}, ensuring that $\mathbb{Q}$ remains a transition rate matrix. In the bound regime, the particles can transition back to the transition regime through $\mathbb{Q}_{C\to AB}$, which together with $\mathbb{Q}_C$ should also have their combined columns sum to zero. This implies that the matrix $\mathbb{Q}_C$ is a renormalized version of the one in Eq. S17.

From a practical point of view, it is unlikely that one could accurately extract these rate functions in the transition region from MD data. However, one can be less ambitious and try to extract a piecewise constant approximation of these rate functions. This requires deriving a smart discretization of the six dimensional space spanned by x_{AB}; one possible discretization is the one presented in the methods section.

B. Parametrization of the MSM/RD scheme using MD trajectories

The MSM/RD scheme requires parametrizing two MSMs. One for the non-interacting regime and one for the transition and bound regimes together. The MSMs for the non-interacting regime can be obtained with standard techniques (17). In the examples in this work, the MSMs for the non-interacting regime are trivial since we already know their form from the benchmark MD model. Thus, we focus on parametrizing the MSM/RD for the transition and bound regime.

All the MSM/RD schemes in this paper are parametrized with the following setup: we only allow two molecules in the system, each molecule is assumed to have a diameter of 5nm, which is the same order of magnitude as some real proteins. The simulation box is a cube with an edge-length of 25nm and periodic boundaries. Each simulation runs for 6×10^6 time steps of $1\times10^{-5}\mu s$ each, yielding a total simulation time of $60\mu s$. We run 600 of these simulations independently, and we use them to parametrize the MSM/RD schemes following the steps below.

To parametrize the MSM/RD scheme, we require a piecewise constant discretization of the transition rate matrix $\mathbb{Q}(x)$. In the numerical algorithm, it was more convenient to use discrete-time MSMs; we will need two discrete-time MSMs to approximate $\mathbb{Q}(x)$. The first one is to approximate the independent dynamics $\mathbb{Q}_A \oplus \mathbb{Q}_B$ in the non-interacting regime, and the second is to approximate the dynamics $\mathbb{Q}(x)$ in the bound and transition regime. The first MSM can be inferred by approximating $\mathbb{Q}_A$ and $\mathbb{Q}_B$ from MD simulations of molecules A and B, each simulated independently and following standard procedures (14–16). The second MSM requires discretizing the MD trajectories of the joint system and then using these discrete trajectories to derive an MSM. The discretization and derivation is as follows:

Discretization of MD trajectories.

1. If in the non-interacting regime, assign a unique unbound state (we use zero).
2. If in the transition regime, assign the corresponding transition state, as defined in Fig.2b.
3. If in the bound regime, use the core-MSM approach (3, 15): if the particles are in a bound state, assign the corresponding bound state; if they are not in a bound state, assign the value of the last transition state or bound state visited.

Derivation of the MSM.

1. Slice discrete trajectories by removing the unbound state.
2. Stitch the trajectories randomly by joining a trajectory that ends in a given state and stitching to another one that begins with that state.
3. Use the stitched discrete trajectories to generate an MSM that can transition between all the bound states and all the transition states. We employ standard inference techniques (17), and we use the PyEMMA software (14) to obtain the MSM and the corresponding implied time-scales. Observing the implied time-scales, we can choose an adequate lagtime for the MSM (17).

The resulting MSM, approximates the full $\mathbb{Q}(x)$ matrix in the transition and bound regime. The two MSMs derived here can be used directly with the Algorithm S.1. In Appendix B, we show the steps to parametrize the MSM/RD scheme for specific simulations. In addition, the translational and rotational diffusion coefficients can be obtained from the MD simulations following standard procedures (6–10, 12).

Below, we show the specific steps to parametrize the MSM/RD scheme from MD trajectories containing the position and orientation of the molecules at every 25^{th} time step. We illustrate these steps for the protein-protein system from Section , and we show the minor variations needed for the dimer system from Section and for the multiparticle implementation.

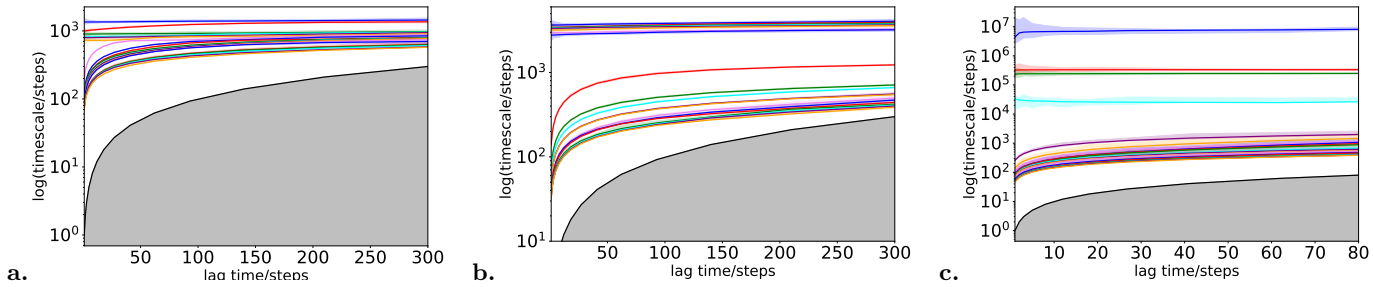


Fig. S.1. Implied time-scales of MSMs including all the bound states and transition states. **a.** Implied time-scales of the protein-protein system from Section . **b.** Implied time-scales of the dimer system from Section . **c.** Implied time-scales of the dimer system used for the multiparticle MSM/RD from Section .

Algorithm S.1 Main algorithm for the MSM/RD scheme. Note the MSMs used in the algorithm use a constant δt to avoid synchronization issues. This is particularly convenient since we will use discrete-time MSM in our implementations with lag-times that are multiples of the simulation time step. It is possible to modify the algorithm to use continuous-time MSMs and propagate them with a Gillespie algorithm.

Input: position and orientation of molecule A and molecule B, maximum time T, time step δt.

- While $t < T$:

  1. Calculate relative position r_{AB} and relative orientation θ_{AB}; and get current regime.
  2. If in non-interacting regime:
     (a) Propagate MSM by δt using the transition rate matrix $\mathbb{Q}_{AB} = \mathbb{Q}_A \oplus \mathbb{Q}_B$, or $\mathbb{Q}_A$ and $\mathbb{Q}_B$ independently.
     (b) Propagate diffusion by δt following Eq. 7 with $k = A, B$.
     (c) If $\|r_{AB}\| < R$: switch to transition regime
  3. Else if in transition regime:
     (a) Propagate MSM by δt using the piecewise constant approximation of the transition rate matrices $\mathbb{Q}_{AB}$ and $\mathbb{Q}_{AB\to C}$.
     (b) If transition towards a bound state C happened:
        i. Switch to bound regime
        ii. Set position and orientation of C compound as average between A and B.
     (c) Else:
        i. Propagate diffusion by δt following Eq. 7 with $k = A, B$.
        ii. If $\|r_{AB}\| \geq R$: switch to non-interacting regime
  4. Else if in bound regime:
     (a) Propagate MSM by δt using the transition rate matrices $\mathbb{Q}_C$ and $\mathbb{Q}_{C\to AB}$.
     (b) If transition towards an unbound transition state happened:
        i. Switch to transition regime
        ii. Set position and orientation of A and B corresponding to the unbound transition state.
     (c) Else:
        i. Propagate diffusion by δt following Eq. 9.
  5. Set $t \leftarrow t + \delta t$

Algorithm S.2 Main algorithm for multiparticle MSM/RD scheme. It is a modified version of Algorithm S.1. Particle compounds refer to a set of particles that are bound together. The compound has its own position and orientation. The particles positions and orientations are assigned relative to those of the particle compound. Also note each possible pair of particles has a regime associated to it.

Input: position and orientation of all molecules, maximum time T, time step δt.

- While $t < T$:

  For all possible pairs of particles (we label a pair as particle A and particle B):

  1. Calculate relative position r_{AB} and relative orientation θ_{AB}; and get current regime.
  2. If in non-interacting regime, apply step 2 from Algorithm S.1.
  3. Else if in transition regime:
     (a) Propagate MSM by δt using the piecewise constant approximation of the transition rate matrices $\mathbb{Q}_{AB}$ and $\mathbb{Q}_{AB\to C}$.
     (b) If transition towards a bound state C happened and transition is allowed (bound site not yet occupied):
        i. If both particles don't belong to any compound: create bound compound with particles A and B.
        ii. Else if only one particle belongs to a compound: bind particle to existing compound.
        iii. Else: bind compounds together (particles belong each to a different compound).
        iv. Switch to bound regime
        v. If new compound was formed: assign it a position and orientation (can be an average between the particles involved, or the corresponding center of a ring molecule)
        vi. For new particles in compound: fix relative position and orientation with respect to the compound's position and orientation.
     (c) Else:
        i. For particles not belonging to a compound: propagate diffusion by δt following Eq. 7
        ii. If $\|r_{AB}\| \geq R$: switch to non-interacting regime

  For all particle compounds: (bound regime)

  1. Calculate transitions within δt in the compound using $\mathbb{Q}_C$ and $\mathbb{Q}_{C\to AB}$ from the two particle MSM (careful to only calculate one possible transition per binding).
  2. If transition towards an unbound transition state happened:
     (a) Split compound and switch the corresponding pair of particles to the transition regime.
     (b) Set position and orientation of particles/compounds corresponding to the unbound transition state.
  3. Else:
     (a) Propagate diffusion by δt following Eq. 9 and using the diffusion coefficients for the corresponding compound (see Appendix D).
     (b) Update the positions and orientations of particles in compound.

  Set $t \leftarrow t + \delta t$

B.1. Protein-protein system:. To parametrize the rates in the transition regime, we collapsed the two conformations of B into one state to yield averaged rates over the two conformations. However, for more complex protein-protein systems, the framework can handle conformation switching in the transition regime.

1. Obtain MD trajectories (position and orientation) from the 600 simulations with a stride of 25 time steps.
2. Define the six bound states around the position and orientation defined in Fig. 4a.
3. Define bound, transition and unbound regime with $\sigma < \|r_{AB}\| < R$; a reasonable choice for our interaction potential is $\sigma = 6.25$nm and $R = 11.25$nm.
4. Define transition states in the transition regime by discretizing the relative position r_{AB} and orientation θ_{AB} between the two molecules in the transition regime. Using Fig. 2 as reference, we discretize r_{AB} in 6 sections and θ_{AB} into 19 sections, yielding total of 114 transition states.
5. Discretize the MD trajectories using the bound states, the transition states and the unbound state, which is defined if the particles are in the non-interacting regime. If the particles are in the bound regime but not in a bound state, use the core MSM approach (15), where the state remains the same as the previous state until a new state is reached.
6. Slice discrete trajectories by removing the unbound state.
7. Stitch the trajectories randomly by joining a trajectory that ends in a given state and stitching to another one that begins with that state.
8. Use the stitched discrete trajectories to generate an MSM that can transition between all the bound states and all the transition states. We employ standard inference techniques (17), and we use the PyEMMA software (14) to obtain the MSM and the corresponding implied time-scales. Observing the implied time-scales, we can choose an adequate lagtime for the MSM, which in this case is of 150 data points/steps or 3750 time steps or $0.0375\mu s$, see Fig. S.1a.
9. Incorporate the obtained MSM into the MSM/RD simulation scheme illustrated in Algorithm S.1.

B.2. Dimer system:. We follow the same steps as in the protein-protein case, except for steps 4 and 8.

Step 4: Define transition states in the transition regime by discretizing the relative position r_{AB} and orientation θ_{AB} between the two molecules in the transition regime. Using Fig. 2 as reference, we discretize r_{AB} in 7 sections and θ_{AB} into 29 sections, yielding total of 203 transition states.

Step 8: Same as step 8 before. However the implied time-scales figure is Fig. S.1b.

B.3. Multiparticle system:. We follow the same steps as in the dimer system, except for step 8.

Step 8: Same as step 8 before. However the implied time-scales figure is Fig. S.1c.

C. MSM/RD algorithms

In algorithm S.1, we present a general outline of the scheme to simulate MSM/RD. We assume we have already derived a piecewise constant discretization of the transition rate matrix $\mathbb{Q}(x)$ or of its discrete-time analog in the three regimes. As this is essentially a numerical scheme to solve Eq. 5, it is possible to discretize it in several different ways, yielding each a different scheme. Nonetheless, they all follow a similar logic. Thus, we present below a simple scheme; while not necessarily the most accurate nor the most efficient, it clearly illustrates the logic behind the method. Note we don't show how to numerically propagate neither the diffusion nor the MSM. This can be done with several standard methods. In Algorithm S.2, we further extend the algorithm to handle multiple particles, as implemented in this paper.

D. Estimation of diffusion coefficients

As both the benchmark and the MSM/RD simulation use the same model for diffusion, the diffusion coefficients of compounds are only relevant for the multiparticle example. To accurately model these multiparticle compounds with MSM/RD, we estimate the translational and rotational diffusion coefficients, D and D^{rot} of the compound formed by two, three, four and five molecules. We assume anisotropic rotational diffusion, and we estimate these coefficients by measuring the mean square displacement at different lag times and applying a linear fit (12). Assuming the position of the center of the compound at time t is $r(t)$, and its orientation is given by the quaternion $\theta(t) = \{s, p\}$, on sufficiently long time scales, the diffusion coefficients follow these relations (10, 12)

$$\left\langle (r(t+\tau) - r(t))^2 \right\rangle = 6D\tau$$
$$\left\langle (p(t+\tau) - p(t))^2 \right\rangle = \frac{3}{4}\left(1 - e^{-2D^{\mathrm{rot}}\tau}\right) \approx \frac{3}{2}D^{\mathrm{rot}}\tau.$$

There are more accurate and sophisticated methods to estimate the diffusion coefficients (11). For more complex cases, it is also possible to include anisotropic translational and rotational diffusion by estimating diffusion matrices (10, 13). However, for our purpose a simple linear fit on these expressions provides already an accurate result.

SI references:

1. X Mao, C Yuan, *Stochastic differential equations with Markovian switching.* (Imperial College Press), (2006).
2. G Yin, C Zhu, *Hybrid switching diffusions: properties and applications.* (Springer New York) Vol. 63, (2010).
3. M Dibak, MJ del Razo, D De Sancho, C Schütte, F Noé, MSM/RD: Coupling markov state models of molecular kinetics with reaction-diffusion simulations. *J. Chem. Phys.* **148**, 214107 (2018).
4. R Zwanzig, Nonlinear generalized langevin equations. *J. Stat. Phys.* **9**, 215–220 (1973).
5. G Ford, M Kac, P Mazur, Statistical mechanics of assemblies of coupled oscillators. *J. Math. Phys.* **6**, 504–515 (1965).
6. D Kleinhans, R Friedrich, A Nawroth, J Peinke, An iterative procedure for the estimation of drift and diffusion coefficients of langevin processes. *Phys. Lett. A* **346**, 42–46 (2005).
7. BP Rao, *Statistical inference for diffusion type processes.* (Arnold London) Vol. 355, (1999).
8. YA Kutoyants, *Statistical inference for ergodic diffusion processes.* (Springer Science & Business Media), (2013).
9. H Sørensen, Parametric inference for diffusion processes observed at discrete points in time: a survey. *Int. Stat. Rev.* **72**, 337–354 (2004).
10. M Linke, J Köfinger, G Hummer, Fully anisotropic rotational diffusion tensor from molecular dynamics simulations. *J. Phys. Chem. B* **122**, 5630–5639 (2018).
11. JT Bullerjahn, S von Bülow, G Hummer, Optimal estimates of self-diffusion coefficients from molecular dynamics simulations. *J. Chem. Phys.* **153**, 024116 (2020).
12. H Qian, MP Sheetz, EL Elson, Single particle tracking. analysis of diffusion and flow in two-dimensional systems. *Biophys. J.* **60**, 910–921 (1991).
13. J Schluttig, D Alamanova, V Helms, US Schwarz, Dynamics of protein-protein encounter: A langevin equation approach with reaction patches. *J. Chem. Phys.* **129**, 10B616 (2008).
14. MK Scherer, et al., PyEMMA 2: A software package for estimation, validation and analysis of Markov models. *J. Chem. Theory Comput.* **11**, 5525–5542 (2015).
15. C Schütte, F Noé, J Lu, M Sarich, E Vanden-Eijnden, Markov state models based on milestoning. *J. Chem. Phys.* **134**, 204105 (2011).
16. JH Prinz, BG Keller, F Noé, Probing molecular kinetics with markov models: Metastable states, transition pathways and spectroscopic observables. *Phys. Chem. Chem. Phys.* **13**, 16912–16927 (2011).
17. JH Prinz, et al., Markov models of molecular kinetics: Generation and validation. *J. Chem. Phys.* **134**, 174105 (2011).